

## 1 **Viral dynamics of SARS-CoV-2 variants in vaccinated and unvaccinated individuals**

2  
3 Stephen M. Kissler\*<sup>1</sup>, Joseph R. Fauver\*<sup>2</sup>, Christina Mack\*<sup>3,4</sup>, Caroline G. Tai<sup>3</sup>, Mallery I.  
4 Breban<sup>2</sup>, Anne E. Watkins<sup>2</sup>, Radhika M. Samant<sup>3</sup>, Deverick J. Anderson<sup>5</sup>, Jessica Metti<sup>6</sup>, Gaurav  
5 Khullar<sup>6</sup>, Rachel Baits<sup>6</sup>, Matthew MacKay<sup>6</sup>, Daisy Salgado<sup>6</sup>, Tim Baker<sup>6</sup>, Joel T. Dudley<sup>6</sup>, Chris-  
6 topher E. Mason<sup>6</sup>, David D. Ho<sup>7</sup>, Nathan D. Grubaugh<sup>†2</sup>, Yonatan H. Grad<sup>†1</sup>

7  
8 <sup>1</sup> Department of Immunology and Infectious Diseases, Harvard T.H. Chan School of Public  
9 Health, Boston, MA

10 <sup>2</sup> Department of Epidemiology of Microbial Diseases, Yale School of Public Health, New Haven,  
11 CT

12 <sup>3</sup> IQVIA, Real World Solutions, Durham, NC

13 <sup>4</sup> Department of Epidemiology, University of North Carolina-Chapel Hill, Chapel Hill, NC

14 <sup>5</sup> Duke Center for Antimicrobial Stewardship and Infection Prevention, Durham, NC

15 <sup>6</sup> TEMPUS Labs, Chicago, IL

16 <sup>7</sup> Aaron Diamond AIDS Research Center, Columbia University Vagelos College of Physicians  
17 and Surgeons, New York, NY

18  
19  
20 \* denotes equal contribution

21 † denotes co-senior authorship

22  
23 Correspondence and requests for materials should be addressed to:

24 Email: [ygrad@hsph.harvard.edu](mailto:ygrad@hsph.harvard.edu)

25 Telephone: 617.432.2275

27 **Abstract.**

28

29 **Background.** The alpha and delta SARS-CoV-2 variants have been responsible for major recent  
30 waves of COVID-19 despite increasing vaccination rates. The reasons for the increased trans-  
31 missibility of these variants and for the reduced transmissibility of vaccine breakthrough infections  
32 are unclear.

33

34 **Methods.** We quantified the course of viral proliferation and clearance for 173 individuals with  
35 acute SARS-CoV-2 infections using longitudinal quantitative RT-PCR tests conducted using an-  
36 terior nares/oropharyngeal samples ( $n = 199,941$ ) as part of the National Basketball Association's  
37 (NBA) occupational health program between November 28<sup>th</sup>, 2020, and August 11<sup>th</sup>, 2021. We  
38 measured the duration of viral proliferation and clearance and the peak viral concentration sepa-  
39 rately for individuals infected with alpha, delta, and non-variants of interest/variants of concern  
40 (non-VOI/VOC), and for vaccinated and unvaccinated individuals.

41

42 **Results.** The mean viral trajectories of alpha and delta infections resembled those of non-  
43 VOI/VOC infections. Vaccine breakthrough infections exhibited similar proliferation dynamics as  
44 infections in unvaccinated individuals (mean peak Ct: 20.5, 95% credible interval [19.0, 21.0] vs.  
45 20.7 [19.8, 20.2], and mean proliferation time 3.2 days [2.5, 4.0] vs. 3.5 days [3.0, 4.0]); however,  
46 vaccinated individuals exhibited faster clearance (mean clearance time: 5.5 days [4.6, 6.6] vs. 7.5  
47 days [6.8, 8.2]).

48

49 **Conclusions.** Alpha, delta, and non-VOI/VOC infections feature similar viral trajectories. Acute  
50 infections in vaccinated and unvaccinated people feature similar proliferation and peak Ct, but  
51 vaccinated individuals cleared the infection more quickly. Viral concentrations do not fully explain  
52 the differences in infectiousness between SARS-CoV-2 variants, and mitigation measures are  
53 needed to limit transmission from vaccinated individuals.

54

55 Two opposing forces shaping the COVID-19 pandemic are (1) the emergence of increasingly  
56 transmissible SARS-CoV-2 variants of concern (VOCs) and (2) the uptake of vaccines that pre-  
57 vent infection, protect against severe disease, and reduce transmission. Among the VOCs, of  
58 special interest are the alpha (lineage B.1.1.7) and delta (B.1.617.2, AY.1, AY.2, AY.3, and  
59 AY.3.1) variants, responsible for recent waves of COVID-19.<sup>1</sup> These variants feature mutations  
60 in the spike protein receptor binding domain<sup>2</sup> that may enhance ACE-2 binding,<sup>3</sup> thus increasing  
61 the efficiency of virus transmission. In addition to, and perhaps due to, these attributes, the viral  
62 trajectories for infections with alpha and delta could feature a higher peak viral load or longer  
63 duration of carriage, both of which could increase transmissibility. Meanwhile, preliminary evi-  
64 dence suggests that individuals with vaccine breakthrough infections are less likely to transmit,<sup>4,5</sup>  
65 but whether this is attributable to lower peak viral loads, shorter duration of carriage, or both,  
66 remains uncertain.

67  
68 By measuring viral concentration over the course of acute infection, it is possible to inform hy-  
69 potheses about the mechanisms that underlie variation in transmissibility. Recent evidence sug-  
70 gests that delta-variant infections may feature substantially higher peak viral concentrations rela-  
71 tive to other lineages,<sup>6</sup> while viral concentrations in alpha-variant infections were indistinguishable  
72 from non-variant infections.<sup>7</sup> Vaccinated individuals who become infected with SARS-CoV-2 may  
73 clear their infections more quickly than unvaccinated individuals,<sup>8</sup> and vaccine breakthrough in-  
74 fections with delta may feature similar peak viral concentrations as non-breakthrough delta infec-  
75 tions.<sup>9</sup> However, many of these studies rely on cross-sectional viral concentration measurements  
76 triggered by the onset of symptoms, which miss viral dynamics during the critical early stages of  
77 infection. Furthermore, population transmission dynamics can bias cross-sectional viral concen-  
78 tration measurements,<sup>10</sup> making it difficult to compare viral concentrations between variants that  
79 emerged at different periods of the pandemic.

80  
81 To overcome these limitations, we collected and analyzed a prospective, longitudinal set of  
82 SARS-CoV-2 viral samples from 173 individuals obtained as part of the National Basketball As-  
83 sociation's occupational health program. Using a Bayesian hierarchical statistical model, we com-  
84 pared SARS-CoV-2 viral dynamics between individuals infected with alpha, delta, and non-vari-  
85 ants of interest/variants of concern (non-VOI/VOCs) as well as for vaccinated and unvaccinated  
86 individuals.

87

## 88 **Methods.**

89

90 Study design. The data reported here represent a convenience sample including team staff,  
91 players, arena staff, and other vendors (e.g., transportation, facilities maintenance, and food  
92 preparation) affiliated with the National Basketball Association (NBA). The study period ran be-  
93 tween November 28<sup>th</sup>, 2020, and August 11<sup>th</sup>, 2021. Clinical samples were obtained by combined  
94 swabs of the anterior nares and oropharynx administered by a trained provider. Viral  
95 concentration was measured using the cycle threshold (Ct) according to the Roche cobas target  
96 1 assay. Ct values were converted to viral genome equivalents using a standard curve  
97 **(Supplementary methods).**

98

99 Study oversight. In accordance with the guidelines of the Yale Human Investigations Committee,  
100 this work with de-identified samples was approved for research not involving human subjects by  
101 the Yale Institutional Review Board (HIC protocol # 2000028599). This project was designated  
102 exempt by the Harvard Institutional Review Board (IRB20-1407).

103

104 Study participants. Out of an initial pool of 872 participants who tested positive for SARS-CoV-2  
105 infection during the study period, 173 individuals (90% male) had clinically confirmed novel  
106 infections that met our inclusion criteria: at least three positive PCR tests (Ct < 40), at least one  
107 negative PCR test (Ct = 40), and at least one test with Ct < 32 with the first positive test (Ct < 40)  
108 occurring before August 1<sup>st</sup> to ensure full sampling of the trajectory before the end of the study  
109 period. (**Table 1**). A total of 19,941 samples were available for this cohort, averaging 548 samples  
110 per week. Of the individuals who met the inclusion criteria, 36 were infected with alpha (B.1.1.7)  
111 and 36 with delta (B.1.617.2, AY.1, AY.2, AY.3, or AY.3.1), as confirmed by sequencing. An  
112 additional 28 individuals were infected with other variants of interest/variants of concern. There  
113 were 37 individuals with vaccine breakthrough infections, defined as infections for which the first  
114 positive test occurred at least two weeks after receipt of the final dose. Of these, 23 received the  
115 Pfizer-BioNTech vaccine, 8 received the Johnson & Johnson/Janssen vaccine, and 3 received  
116 the Moderna vaccine. The vaccine manufacturer was not reported for the remaining 3 individuals.

117

118 Study outcomes. We quantified the viral proliferation duration (time from first possible detection  
119 to peak viral concentration) the viral clearance duration (time from peak viral concentration to  
120 clearance of acute infection), the duration of acute infection (proliferation duration plus clearance

121 duration), and the peak viral concentration for each person. We also quantified the population  
122 mean values of these quantities separately for individuals infected with alpha ( $n = 36$ ), delta ( $n =$   
123  $36$ ), and non-VOI/VOCs ( $n = 41$ ), as well as for vaccinated ( $n = 37$ ) and unvaccinated ( $n = 136$ )  
124 individuals.

125  
126 Genome sequencing and lineage assignments. RNA was extracted and confirmed as SARS-CoV-  
127 2 positive by RT-qPCR with the Thermo Fisher TaqPath SARS-CoV-2 assay.<sup>11</sup> Next Generation  
128 Sequencing with the Illumina COVIDSeq ARTIC primer set<sup>12</sup> was used for viral amplification. Li-  
129 brary preparation was performed using the amplicon-based Illumina COVIDseq Test v03<sup>13</sup> and  
130 sequenced 2x74 on Illumina NextSeq 550 following the protocol as described in Illumina's docu-  
131 mentation.<sup>14</sup> The resulting FASTQs were processed and analyzed on Illumina BaseSpace Labs  
132 using the Illumina DRAGEN COVID Lineage Application;<sup>15</sup> versions included are 3.5.0, 3.5.1,  
133 3.5.2, and 3.5.3. The DRAGEN COVID Lineage pipeline was run with default parameters recom-  
134 mended by Illumina. Samples were considered SARS-COV-2 positive if at least 5 viral amplicon  
135 targets were detected at 20x coverage. Each SARS-COV-2 positive sample underwent lineage  
136 assignment and phylogenetics analysis using the most updated version of Pangolin<sup>16</sup> and  
137 NextClade,<sup>17</sup> respectively.

138  
139 Statistical analysis. Following previously described methods,<sup>18</sup> we used a Bayesian hierarchical  
140 model to estimate the proliferation duration, clearance duration, and peak viral concentration for  
141 each person and for the sub-populations of interest. The model describes the  $\log_{10}$  viral concen-  
142 tration during an acute infection using a continuous piecewise-linear curve with control points that  
143 specify the time of acute infection onset, the time and magnitude of peak viral concentration, and  
144 the time of acute infection clearance. The assumption of piecewise linearity is equivalent to as-  
145 suming exponential viral growth during the proliferation period followed by exponential viral decay  
146 during the clearance period. The control points were inferred using the Hamiltonian Monte Carlo  
147 algorithm as implemented in Stan (version 2.24).<sup>19</sup> We used priors informed by a previous  
148 analysis<sup>18</sup> for the main analysis and conducted a sensitivity analysis using vague priors as well  
149 as a strongly biased set of priors to assess robustness to the choice of prior. Full details are given  
150 in the **Supplementary methods**. Data and code are available online.<sup>20</sup>

151

152 **Results.**

153 Summary of viral concentration measurements and model fit. A median of 6 samples (IQR: [4, 9])  
154 with Ct values that surpassed the limit of detection (Ct = 40) were recorded for each person. The  
155 raw viral concentration measurements are depicted in **Figure 1** for individuals infected with alpha,  
156 delta, and non-VOI/VOCs as well as for unvaccinated and vaccinated infected individuals. Many  
157 of the tail samples depicted in **Figure 1** reflect samples with high Ct value/low viral concentration  
158 after the conclusion of acute infection. As these were not the main object of study in this analysis,  
159 any tests that occurred after the conclusion of an individual's acute infection (as specified by the  
160 statistical model) are depicted in lighter shades. Visually, the trajectories appear similar across  
161 variants and vaccination statuses. While there are fewer low-level positives following acute infec-  
162 tion for those with vaccine breakthrough and delta infections, this may reflect the fact that delta  
163 and breakthrough infections were more likely to occur near the end of the study period, which  
164 may have led to censoring of these points, as well as the substantial overlap in these categories  
165 (see **Table 1**). The individual-level model fits are depicted **Supplementary Figures 1-9**. The  
166 Gelman R-hat statistic<sup>21</sup> was less than 1.1 for all parameters, indicating good convergence. There  
167 were no divergent iterations, indicating good exploration of the parameter space.

168  
169 Viral trajectories by variant. We found no difference in the mean peak viral concentration, prolif-  
170 eration duration, clearance duration, or duration of acute infection for alpha or delta relative to  
171 non-VOI/VOCs, as evidenced by overlapping 95% credible intervals (**Figure 2A-F, Supplemen-**  
172 **tary Table 1**). However, delta infections featured more frequent low peak Ct values, and corre-  
173 sponding high peak viral concentrations, than alpha or non-VOI/VOC infections, with 13.0% of  
174 the posterior delta trajectories surpassing a Ct value of 15 (9.6 log<sub>10</sub> RNA copies/ml) vs. 6.9% and  
175 10.2% of the posterior alpha and non-VOI/VOC trajectories surpassing the same threshold (**Fig-**  
176 **ure 2G**). For those infected with delta, there is some evidence that vaccinated individuals tended  
177 to clear the virus more quickly than unvaccinated individuals (mean 5.9 days (95% credible inter-  
178 val [4.8, 7.2]) in vaccinated individuals vs. 7.6 days [5.5, 10.1] in unvaccinated individuals; **Sup-**  
179 **plementary Figure 10**), though the sample sizes are small and the 95% credible intervals for the  
180 mean clearance duration overlap.

181  
182 Viral trajectories by vaccination status. We found no difference in the mean peak viral concentra-  
183 tion or proliferation duration between vaccinated and unvaccinated individuals as evidenced by  
184 overlapping 95% credible intervals (**Figure 3**). However, breakthrough infections featured a faster  
185 clearance time (mean 5.5 days [4.6, 6.5] vs. 7.5 days [6.8, 8.2] in unvaccinated individuals),

186 leading to a shorter overall duration of infection (8.7 days [7.6, 9.9] in vaccinated individuals vs.  
187 11.0 days [10.3, 11.8] in unvaccinated individuals). We found no difference in viral trajectories for  
188 infected individuals who received the Pfizer-BioNTech vaccine ( $n = 23$ ) vs. the Johnson & John-  
189 son/Janssen vaccine ( $n = 8$ ; **Supplementary Figure 11**). We did not assess viral trajectories for  
190 breakthrough infections in individuals who received the Moderna vaccine due to the small sample  
191 size ( $n = 3$ ).

192

## 193 **Discussion.**

194 With the emergence of more transmissible SARS-CoV-2 variants such as alpha and delta, a key  
195 goal has been to understand which factors contribute to increased transmissibility. Our results  
196 indicate that the viral dynamics of infections caused by the alpha variant resemble those caused  
197 by the founding SARS-CoV-2 lineages, with similar proliferation and clearance times and similar  
198 peak viral concentrations. Viral dynamics in the oropharynx and nasopharynx therefore do not  
199 explain the elevated transmissibility of the alpha variant relative to the founding SARS-CoV-2  
200 lineages.<sup>22</sup> Instead, other factors, such as enhanced receptor binding which could lower the viral  
201 dose required for infection, may contribute to the alpha variant's increased transmissibility. The  
202 viral dynamics of the delta variant are similar, with the exception that infections caused by the  
203 delta variant appear more likely to feature high peak viral concentrations. It is unclear if the greater  
204 proportion of cases with high peak viral concentrations reflects the underlying biology of the delta  
205 variant, the limited number of cases and sampling, or other factors, including the higher fraction  
206 of delta infections that were in vaccinated individuals. Infections with unusually high peak viral  
207 concentration may play an outsized role in spreading the virus, either by increasing the risk of  
208 transmission outside of close-contact settings<sup>23</sup> or increasing the likelihood of "superspreading"  
209 events, pointing towards a possible mechanism for the enhanced transmissibility of the delta var-  
210 iant. Upper respiratory viral concentrations also do not explain the possible enhanced pathogenic-  
211 ity of the alpha and delta variants.<sup>24</sup> Further studies are needed to uncover the origins of any  
212 differences in virulence, which could stem from differences in systemic viral dynamics that are not  
213 captured by oropharyngeal/nasopharyngeal samples.

214

215 A second key objective is to define the impact of COVID-19 vaccines on viral dynamics. Strong  
216 evidence demonstrates that each of the vaccines used by individuals in this cohort—the Pfizer/Bi-  
217 oNTech, Moderna, and Johnson & Johnson/Janssen vaccines—reduces the rates of symptomatic  
218 COVID-19.<sup>25–27</sup> A growing body of data also suggests that these vaccines reduce rates of



219 asymptomatic infection.<sup>28–30</sup> The extent to which infected vaccinated people can transmit SARS-  
220 CoV-2 has been unclear, with recent data supporting that breakthrough infections are infectious.<sup>9</sup>  
221 Our data and a recent report from Singapore<sup>8</sup> show that vaccine breakthrough cases follow a  
222 similar proliferation phase and reach similar peak viral concentrations as unvaccinated cases, but  
223 have a more rapid clearance phase, thereby modestly shortening the overall duration of infection.  
224 If the Ct values in vaccinated and unvaccinated infected individuals reflect the same amounts of  
225 infectious virus, then this implies that individuals with breakthrough infections may be as infectious  
226 as unvaccinated individuals in the early stage of the infection, but remain infectious for a shorter  
227 time, reducing the total degree of onward transmission. These findings are in keeping with the  
228 hypothesis that vaccination protects against the severe manifestations of disease but offers less  
229 protection against infection in the upper airway. Precautions are therefore necessary to prevent  
230 onward transmission even from vaccinated individuals.

231  
232 Our ability to detect differences in SARS-CoV-2 viral dynamics between key populations was  
233 limited by small sample sizes and a high degree of interpersonal variation. More prospective lon-  
234 gitudinal testing data within diverse cohorts is urgently needed to help resolve these patterns,  
235 particularly the peak viral concentration distribution for delta infections. The participants in this  
236 study were predominately young, male, and healthy, and therefore not representative across the  
237 general population. This underscores the need for similar studies in more diverse cohorts. Symp-  
238 toms were not tracked throughout infection in this observational cohort; we were unable to assess  
239 differences in viral dynamics between symptomatic and asymptomatic individuals, nor were we  
240 able to link the timing of symptoms with key points in the viral trajectories. We did not test for the  
241 presence of infectious virus. While high viral concentrations are associated with elevated infec-  
242 tiousness,<sup>31</sup> the nature of this association may be influenced by multiple factors, including variant,  
243 vaccination status, immune function, and host genetics.<sup>32</sup> Viral culture studies and patient data  
244 would therefore help to contextualize the findings presented in this study.

245  
246 This study provides a detailed picture of acute SARS-CoV-2 viral dynamics for key variants of  
247 concern in vaccinated and unvaccinated individuals. Frequent longitudinal measurements of viral  
248 concentrations can play a valuable role in illuminating factors contributing to SARS-CoV-2 trans-  
249 missibility and the nature and extent of the impact of vaccination on viral dynamics in acute infec-  
250 tions, thus informing interventions needed to mitigate the impact of COVID-19.

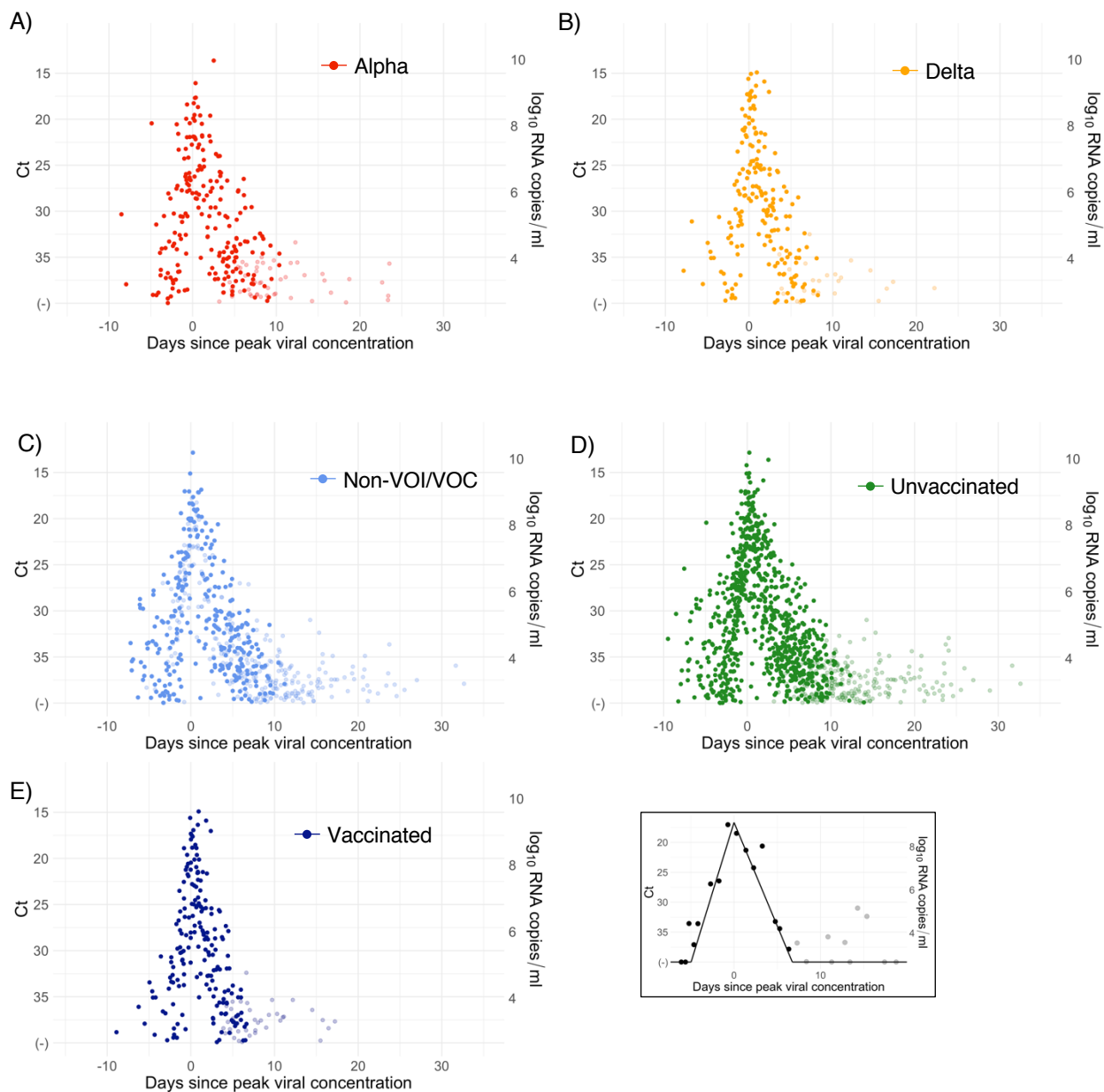
251



	Alpha (%)	Delta (%)	Other VOI/VVOC (%)	Non- VOI/VOC (%)	Not genotyped (%)	Total (%)
<b>Total</b>	36 (20.8)	36 (20.8)	28 (16.2)	41 (23.7)	32 (18.5)	173 (100)
<b>Age</b>						
<18	3 (1.7)	2 (1.2)	2 (1.2)	0 (0)	1 (0.6)	8 (4.6)
18-29	23 (13.3)	6 (3.5)	13 (7.5)	26 (15)	11 (6.4)	79 (45.7)
30-39	4 (2.3)	8 (4.6)	6 (3.5)	7 (4.0)	6 (3.5)	31 (17.9)
40-49	4 (2.3)	14 (8.1)	4 (2.3)	3 (1.7)	5 (2.9)	30 (17.3)
50-59	2 (1.2)	4 (2.3)	1 (0.6)	2 (1.2)	4 (2.3)	13 (7.5)
≥60	0 (0)	2 (1.2)	2 (1.2)	3 (1.7)	5 (2.9)	12 (6.9)
<b>Symptoms reported</b>						
No	18 (10.4)	23 (13.3)	15 (8.7)	22 (12.7)	24 (13.9)	102 (59.0)
Yes	18 (10.4)	13 (7.5)	13 (7.5)	19 (11.0)	8 (4.6)	71 (41.0)
<b>Vaccine breakthrough</b>						
No	32 (18.5)	11 (6.4)	25 (14.5)	41 (23.7)	27 (15.6)	136 (78.6)
Yes	4 (2.3)	25 (14.5)	3 (1.7)	0 (0)	5 (2.9)	37 (21.4)

252  
253  
254  
255  
256

**Table 1. Characteristics of the study population.** Number and percent (in parentheses) of individuals in the study population by age group, reported symptoms, and vaccine breakthrough status, stratified by variant.

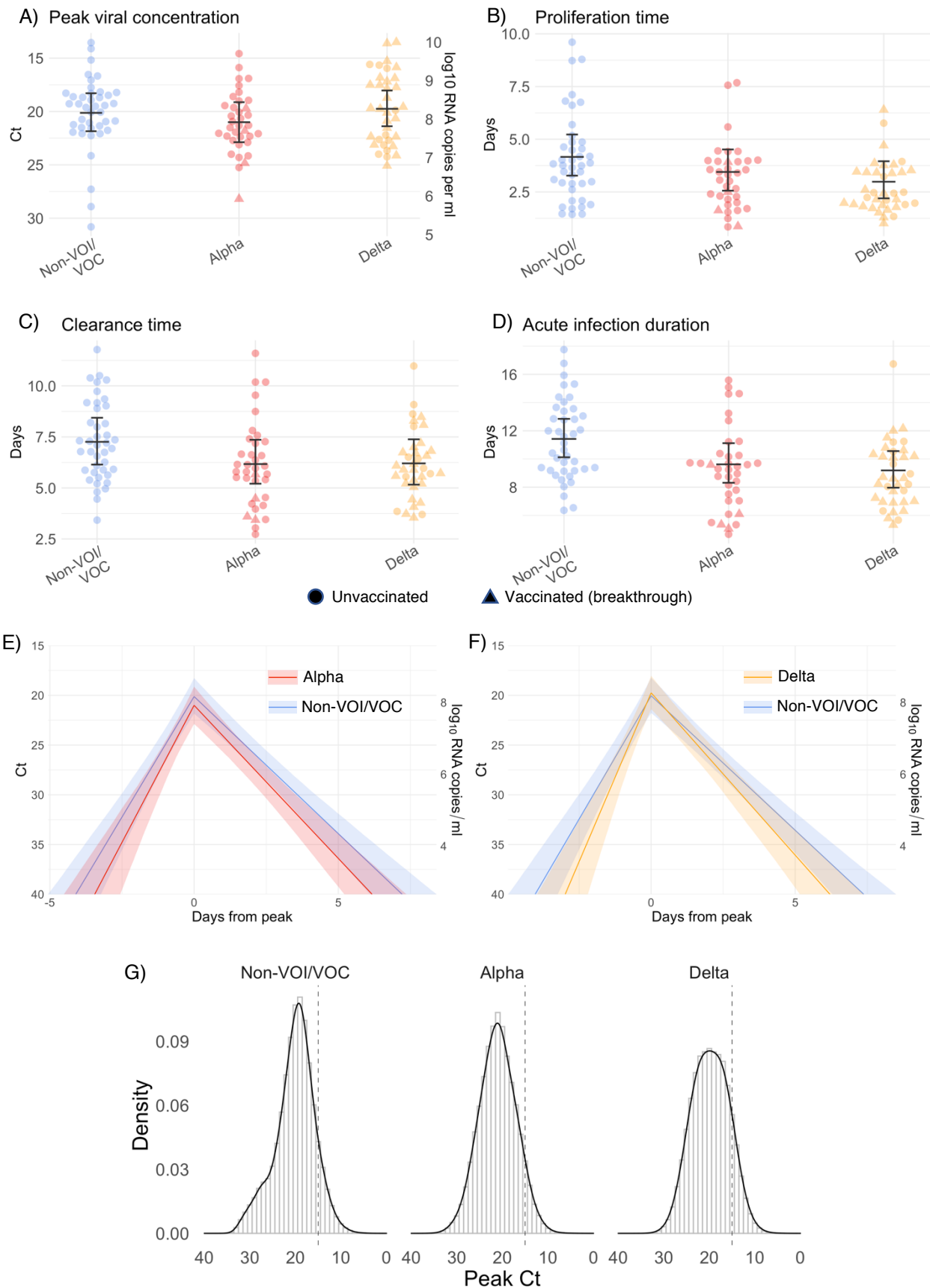


257  
258  
259

260

261  
262

**Figure 1. Raw Ct values by variant and vaccination status.** Raw Ct values (points) for individuals infected with (A) alpha, (B) delta, or (C) non-VOI-VOCs, and for (D) unvaccinated and (E) vaccinated individuals. Points are horizontally aligned so that the inferred mean peak viral concentration for each person occurs at time 0. Points that fall after the conclusion of an individual's acute infection, as measured by the individual's mean posterior infection clearance time, are partially transparent, as these were not the focus of our study. The inset illustrates the process of making the tail points transparent: black points depict viral concentration measurements for a single person and the solid black lines depict the individual's mean posterior viral trajectory.



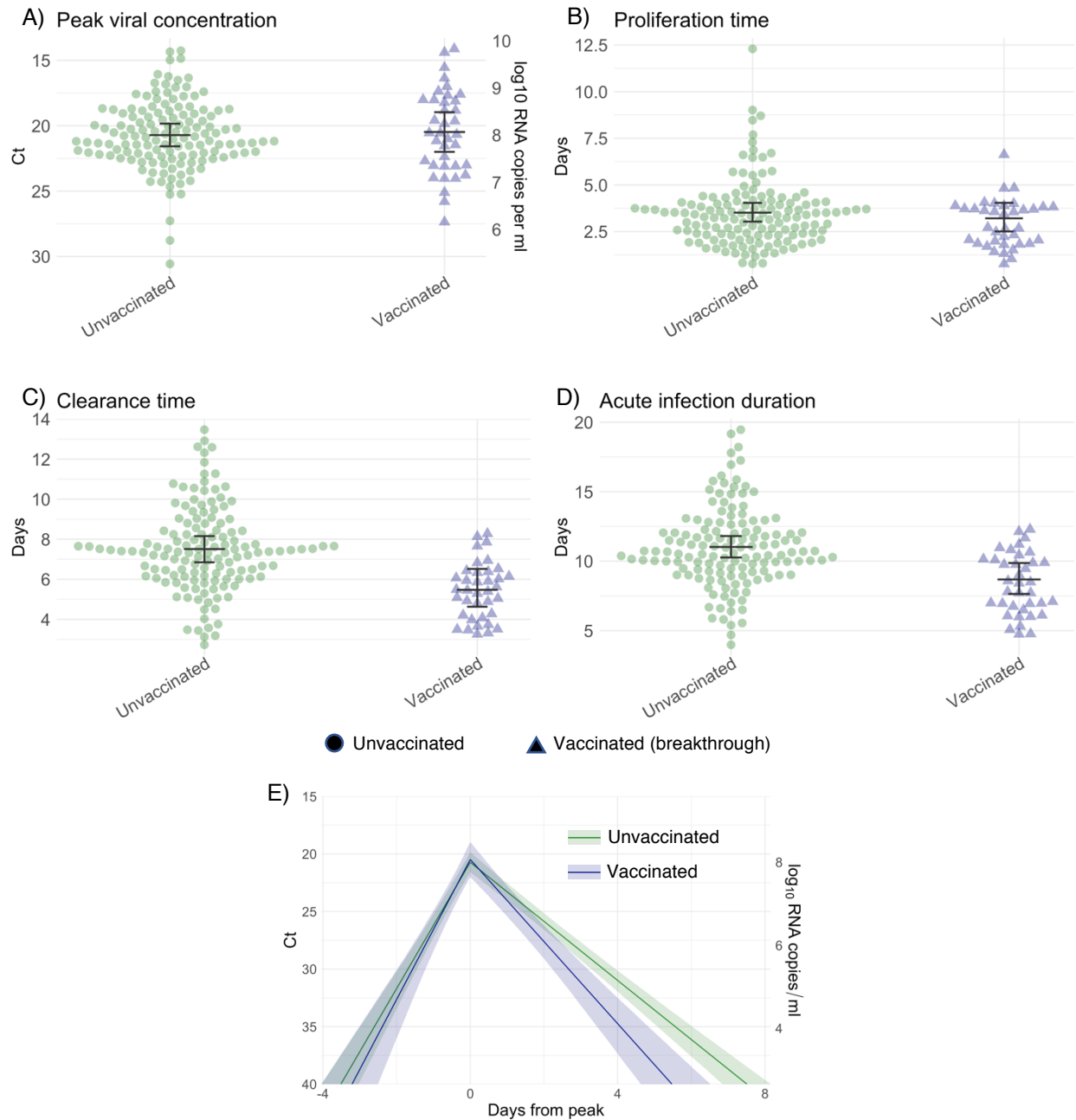
271

272  
273

274  
275

276

277 **Figure 2. Estimated viral trajectory parameters for SARS-CoV-2 variants alpha and delta.** Individual  
278 posterior means (points) with population means and 95% credible intervals (hatched lines) for (A) the peak  
279 viral concentration, (B) the proliferation duration, (C) the clearance duration, and (D) the total duration of  
280 acute infection for individuals infected with a non-VOI/VOC (light blue), alpha (red), or delta (orange). Cir-  
281 cles denote unvaccinated individuals and triangles denote vaccinated individuals (breakthroughs). The  
282 points are jittered horizontally to avoid overlap. Panes (E)-(F) depict the mean posterior viral trajectories for  
283 alpha (E, red) and delta (F, orange) infections relative to non-VOI/VOC infections (light blue), as specified  
284 by the population means and credible intervals in (A)-(D). Solid lines in panes (E)-(F) depict the mean  
285 posterior viral trajectories and shaded regions represent 95% credible areas for the mean posterior trajec-  
286 tories. Histograms in pane (G) depict the posterior distributions of peak Ct values aggregated across all  
287 individuals infected with a non-VOI/VOC, alpha, and delta. The dashed line marks Ct = 15 (9.6 log<sub>10</sub> RNA  
288 copies/ml) to facilitate comparison of the frequency of low peak Ct values/high peak viral concentrations  
289 across variants.  
290



291  
292

293  
294  
295

296  
297

298 **Figure 3. Estimated viral trajectory parameters for SARS-CoV-2 infections in unvaccinated and vac-**  
299 **cinated individuals.** Individual posterior means (points) with population means and 95% credible intervals  
300 (hatched lines) for (A) the peak viral concentration, (B) the proliferation duration, (C) the clearance duration,  
301 and (D) the total duration of acute infection for unvaccinated individuals (green) and vaccinated individuals  
302 (dark blue). Circles denote unvaccinated individuals and triangles denote vaccinated individuals (break-  
303 throughs). The points are jittered horizontally to avoid overlap. Pane (E) depicts the mean posterior viral  
304 trajectories for vaccinated individuals (green) relative to unvaccinated individuals (dark blue), as specified  
305 by the population means and credible intervals in (A)-(D). Solid lines in pane (E) depict the mean posterior  
306 viral trajectories and shaded regions represent 95% credible areas for the mean posterior trajectories.

## 307 References

- 308
- 309 1. Centers for Disease Control and Prevention. COVID Data Tracker. Published 2021. Accessed  
310 May 20, 2021. <https://covid.cdc.gov/covid-data-tracker/>
- 311 2. Galloway SE, Paul P, MacCannell DR, Johansson MA, Brooks JT, MacNeil A, et al. Emergence of  
312 SARS-CoV-2 B.1.1.7 Lineage — United States, December 29, 2020–January 12, 2021. *MMWR*  
313 *Morb Mortal Wkly Rep.* 2021;70(3):95-99. doi:10.15585/mmwr.mm7003e2
- 314 3. Yi C, Sun X, Ye J, Ding L, Liu M, Yang Z, et al. Key residues of the receptor binding motif in the  
315 spike protein of SARS-CoV-2 that interact with ACE2 and neutralizing antibodies. *Cell Mol*  
316 *Immunol.* 2020;17(6):621-630. doi:10.1038/s41423-020-0458-z
- 317 4. Bailly B, Guilpain L, Bouiller K, Chirouze C, N'Debi M, Soulier A, et al. BNT162b2 Messenger RNA  
318 Vaccination Did Not Prevent an Outbreak of Severe Acute Respiratory Syndrome Coronavirus 2  
319 Variant 501Y.V2 in an Elderly Nursing Home but Reduced Transmission and Disease Severity.  
320 *Clin Infect Dis.* Published online May 16, 2021. doi:10.1093/cid/ciab446
- 321 5. Brinkley-Rubinstein L, Peterson M, Martin R, Chan P, Berk J. Breakthrough SARS-CoV-2  
322 Infections in Prison after Vaccination. *N Engl J Med.* Published online July 7,  
323 2021:NEJMc2108479. doi:10.1056/NEJMc2108479
- 324 6. Li B, Deng A, Li K, Hu Y, Li Z, Xiong Q, et al. Viral infection and transmission in a large, well-  
325 traced outbreak caused by the SARS-CoV-2 Delta variant. *medRxiv.* Published online 2021.
- 326 7. Ke R, Martinez PP, Smith RL, Gibson LL, Mirza A, Conte M, et al. Daily sampling of early SARS-  
327 CoV-2 infection reveals substantial heterogeneity in infectiousness. *medRxiv.* Published online  
328 2021. doi:<https://www.medrxiv.org/content/10.1101/2021.07.12.21260208v1>
- 329 8. Chia PY, Ong SWX, Chiew CJ, Ang LW, Chavatte J-M, Mak T-M, et al. Virological and serological  
330 kinetics of SARS-CoV-2 Delta variant vaccine-breakthrough infections: a multi-center cohort study.  
331 *medRxiv.* Published online 2021.
- 332 9. Brown CM, Vostok J, Johnson H, Burns M, Gharpure R, Sami S, et al. Outbreak of SARS-CoV-2  
333 Infections, Including COVID-19 Vaccine Breakthrough Infections, Associated with Large Public  
334 Gatherings — Barnstable County, Massachusetts, July 2021. *MMWR Morb Mortal Wkly Rep.*  
335 2021;70(31):1059-1062. doi:10.15585/mmwr.mm7031e2
- 336 10. Hay JA, Kennedy-Shaffer L, Kanjilal S, Lennon NJ, Gabriel SB, Lipsitch M, et al. Estimating  
337 epidemiologic dynamics from cross-sectional viral load distributions. *Science (80- )*.  
338 2021;373(6552):eabh0635. doi:10.1126/science.abh0635
- 339 11. United States Food and Drug Administration. *Emergency Use Authorization for TaqPath COVID-  
340 19 Combo Kit.*; 2020. <https://www.fda.gov/media/136113/download>
- 341 12. Loman N, Rowe W, Rambaut A. nCoV-2019 novel coronavirus bioinformatics protocol.
- 342 13. Illumina. *Illumina COVIDSeq Test Instructions for Use.*; 2021.  
343 <https://www.fda.gov/media/138776/download>
- 344 14. Illumina. NextSeq 550 System Documentation. Published 2021. Accessed June 10, 2021.  
345 [https://support.illumina.com/sequencing/sequencing\\_instruments/nextseq-550/documentation.html](https://support.illumina.com/sequencing/sequencing_instruments/nextseq-550/documentation.html)
- 346 15. BaseSpace Labs. DRAGEN COVID Lineage. Published online 2021.
- 347 16. Rambaut A, Holmes EC, O'Toole Á, Hill V, McCrone JT, Ruis C, et al. A dynamic nomenclature  
348 proposal for SARS-CoV-2 lineages to assist genomic epidemiology. *Nat Microbiol.*  
349 2020;5(11):1403-1407. doi:10.1038/s41564-020-0770-5
- 350 17. Aksamentov I, Neher R. NextClade. Published 2021. Accessed June 10, 2021.  
351 <https://clades.nextstrain.org/>
- 352 18. Kissler SM, Fauver JR, Mack C, Olesen SW, Tai C, Shiue KY, et al. Viral dynamics of acute  
353 SARS-CoV-2 infection and applications to diagnostic and public health strategies. *PLoS Biol.*  
354 2021;19(7):1-17. doi:10.1371/journal.pbio.3001333
- 355 19. Carpenter B, Gelman A, Hoffman MD, Lee D, Goodrich B, Betancourt M, et al. Stan : A  
356 Probabilistic Programming Language. *J Stat Softw.* 2017;76(1). doi:10.18637/jss.v076.i01
- 357 20. Kissler SM. Github Repository: CtTrajectories\_AllVariants. Published 2021. Accessed June 14,  
358 2021. [https://github.com/gradlab/CtTrajectories\\_AllVariants](https://github.com/gradlab/CtTrajectories_AllVariants)
- 359 21. Gelman A, Carlin JB, Stern HS, Dunson DB, Vehtari A, Rubin DB. *Bayesian Data Analysis.* 3rd ed.



- 360 CRC Press; 2013.
- 361 22. Davies NG, Abbott S, Barnard RC, Jarvis CI, Kucharski AJ, Munday JD, et al. Estimated  
362 transmissibility and impact of SARS-CoV-2 lineage B.1.1.7 in England. *Science* (80- ).  
363 2021;372(6538):eabg3055. doi:10.1126/science.abg3055
- 364 23. Mack CD, Wasserman EB, Perrine CG, MacNeil A, Anderson DJ, Myers E, et al. Implementation  
365 and Evolution of Mitigation Measures, Testing, and Contact Tracing in the National Football  
366 League, August 9–November 21, 2020. *MMWR Morb Mortal Wkly Rep.* 2021;70(4):130-135.  
367 doi:10.15585/mmwr.mm7004e2
- 368 24. Fisman DN, Tuite AR. Progressive Increase in Virulence of Novel SARS-CoV-2 Variants in  
369 Ontario, Canada. *medRxiv*. Published online 2021.
- 370 25. Baden LR, El Sahly HM, Essink B, Kotloff K, Frey S, Novak R, et al. Efficacy and Safety of the  
371 mRNA-1273 SARS-CoV-2 Vaccine. *N Engl J Med.* 2021;384(5):403-416.  
372 doi:10.1056/NEJMoa2035389
- 373 26. Polack FP, Thomas SJ, Kitchin N, Absalon J, Gurtman A, Lockhart S, et al. Safety and Efficacy of  
374 the BNT162b2 mRNA Covid-19 Vaccine. *N Engl J Med.* 2020;383(27):2603-2615.  
375 doi:10.1056/NEJMoa2034577
- 376 27. Oliver SE, Gargano JW, Scobie H, Wallace M, Hadler SC, Leung J, et al. The Advisory Committee  
377 on Immunization Practices' Interim Recommendation for Use of Janssen COVID-19 Vaccine —  
378 United States, February 2021. *MMWR Morb Mortal Wkly Rep.* 2021;70(9):329-332.  
379 doi:10.15585/mmwr.mm7009e4
- 380 28. Andrejko KL, Pry J, Myers JF, Jewell NP, Openshaw J, Watt J, et al. Prevention of COVID-19 by  
381 mRNA-based vaccines within the general population of California. *medRxiv*. Published online  
382 2021.
- 383 29. Corchado-Garcia J, Puyraimond-Zemmour D, Hughes T, Cristea-Platon T, Lenehan P, Pawlowski  
384 C, et al. Real-world effectiveness of Ad26.COVS adenoviral vector vaccine for COVID-19.  
385 *medRxiv*. Published online 2021.
- 386 30. Pawlowski C, Lenehan P, Puranik A, Agarwal V, Venkatakrishnan A, Niesen MJM, et al. FDA-  
387 authorized COVID-19 vaccines are effective per real-world evidence synthesized across a multi-  
388 state health system. *medRxiv*. Published online 2021.
- 389 31. Singanayagam A, Patel M, Charlett A, Lopez Bernal J, Saliba V, Ellis J, et al. Duration of  
390 infectiousness and correlation with RT-PCR cycle threshold values in cases of COVID-19,  
391 England, January to May 2020. *Euro Surveill.* 2020;25(32):1-5. doi:10.2807/1560-  
392 7917.ES.2020.25.32.2001483
- 393 32. Butler D, Mozsary C, Meydan C, Foox J, Rosiene J, Shaiber A, et al. Shotgun transcriptome,  
394 spatial omics, and isothermal profiling of SARS-CoV-2 infection reveals unique host responses,  
395 viral diversification, and drug interactions. *Nat Commun.* 2021;12(1):1660. doi:10.1038/s41467-  
396 021-21361-7
- 397 33. Kudo E, Israelow B, Vogels CBF, Lu P, Wyllie AL, Tokuyama M, et al. Detection of SARS-CoV-2  
398 RNA by multiplex RT-qPCR. Sugden B, ed. *PLOS Biol.* 2020;18(10):e3000867.  
399 doi:10.1371/journal.pbio.3000867
- 400 34. Vogels C, Fauver J, Ott IM, Grubaugh N. *Generation of SARS-COV-2 RNA Transcript Standards*  
401 *for QRT-PCR Detection Assays.*; 2020. doi:10.17504/protocols.io.bdv6i69e
- 402 35. Cleary B, Hay JA, Blumenstiel B, Gabriel S, Regev A, Mina MJ. Efficient prevalence estimation  
403 and infected sample identification with group testing for SARS-CoV-2. *medRxiv*. Published online  
404 2020.
- 405 36. Tom MR, Mina MJ. To Interpret the SARS-CoV-2 Test, Consider the Cycle Threshold Value. *Clin*  
406 *Infect Dis.* 2020;02115(Xx):1-3. doi:10.1093/cid/ciaa619
- 407 37. R Development Core Team R. R: A Language and Environment for Statistical Computing. Team  
408 RDC, ed. *R Found Stat Comput.* 2011;1(2.11.1):409. doi:10.1007/978-3-540-74686-7
- 409 38. Kissler SM, Fauver JR, Mack C, Olesen SW, Tai C, Shiue KY, et al. Viral dynamics of acute  
410 SARS-CoV-2 infection and applications to diagnostic and public health strategies. Riley S, ed.  
411 *PLOS Biol.* 2021;19(7):e3001333. doi:10.1371/journal.pbio.3001333



413 **Supplementary Appendix.**

414

415 Converting Ct values to viral genome equivalents. To convert Ct values to viral genome  
416 equivalents, we first converted the Roche cobas target 1 Ct values to equivalent Ct values on a  
417 multiplexed version of the RT-qPCR assay from the US Centers for Disease Control and  
418 Prevention.<sup>33</sup> We did this following our previously described methods.<sup>18</sup> Briefly, we adjusted the  
419 Ct values using the best-fit linear regression between previously collected Roche cobas target 1  
420 Ct values and CDC multiplex Ct values using the following regression equation:

421

$$422 \quad y_i = \beta_0 + \beta_1 x_i + \epsilon_i \quad (S1)$$

423

424 Here,  $y_i$  denotes the  $i^{\text{th}}$  Ct value from the CDC multiplex assay,  $x_i$  denotes the  $i^{\text{th}}$  Ct value from the  
425 Roche cobas target 1 test, and  $\epsilon_i$  is an error term with mean 0 and constant variance across all  
426 samples. The coefficient values are  $\beta_0 = -6.25$  and  $\beta_1 = 1.34$ .

427

428 Ct values were fitted to a standard curve to convert Ct value data to RNA copies. Synthetic T7  
429 RNA transcripts corresponding to a 1,363 b.p. segment of the SARS-CoV-2 nucleocapsid gene  
430 were serially diluted from  $10^6$ - $10^0$  RNA copies/ $\mu\text{l}$  in duplicate to generate a standard curve<sup>34</sup>  
431 (**Supplementary Table 2**). The average Ct value for each dilution was used to calculate the slope  
432 (-3.60971) and intercept (40.93733) of the linear regression of Ct on  $\log_{10}$  transformed standard  
433 RNA concentration, and Ct values from subsequent RT-qPCR runs were converted to RNA copies  
434 using the following equation:

435

$$436 \quad \log_{10}([\text{RNA}]) = (Ct - 40.93733)/(-3.60971) + \log_{10}(250) \quad (S2)$$

437

438 Here, [RNA] represents the RNA copies /ml. The  $\log_{10}(250)$  term accounts for the extraction (300  
439  $\mu\text{l}$ ) and elution (75  $\mu\text{l}$ ) volumes associated with processing the clinical samples as well as the  
440 1,000  $\mu\text{l}/\text{ml}$  unit conversion.

441

442 Model fitting.

443 For the statistical analysis, we removed any sequences of 3 or more consecutive negative tests  
444 (Ct = 40) to avoid overfitting to these trivial values. Following our previously described methods,<sup>18</sup>  
445 we assumed that the viral concentration trajectories consisted of a proliferation phase, with

446 exponential growth in viral RNA concentration, followed by a clearance phase characterized by  
447 exponential decay in viral RNA concentration.<sup>35</sup> Since Ct values are roughly proportional to the  
448 negative logarithm of viral concentration<sup>36</sup>, this corresponds to a linear decrease in Ct followed by  
449 a linear increase. We therefore constructed a piecewise-linear regression model to estimate the  
450 peak Ct value, the time from infection onset to peak (*i.e.* the duration of the proliferation stage),  
451 and the time from peak to infection resolution (*i.e.* the duration of the clearance stage). The  
452 trajectory may be represented by the equation

$$E[Ct(t)] = \begin{cases} \text{l.o.d.} & t \leq t_o \\ \text{l.o.d.} - \frac{\delta}{t_p - t_o}(t - t_o) & t_o < t \leq t_p \\ \text{l.o.d.} - \delta + \frac{\delta}{t_r - t_p}(t - t_p) & t_p < t \leq t_r \\ \text{l.o.d.} & t > t_r \end{cases} \quad (\text{S3})$$

454  
455  
456 Here,  $E[Ct(t)]$  represents the expected value of the Ct at time  $t$ , “l.o.d” represents the RT-qPCR  
457 limit of detection,  $\delta$  is the absolute difference in Ct between the limit of detection and the peak  
458 (lowest) Ct, and  $t_o$ ,  $t_p$ , and  $t_r$  are the onset, peak, and recovery times, respectively.

459  
460 Before fitting, we re-parametrized the model using the following definitions:

- 461
- 462 •  $\Delta Ct(t) = \text{l.o.d.} - Ct(t)$  is the difference between the limit of detection and the observed Ct
  - 463 value at time  $t$ .
  - 464 •  $\omega_p = t_p - t_o$  is the duration of the proliferation stage.
  - 465 •  $\omega_r = t_r - t_p$  is the duration of the clearance stage.
- 466

467 We constrained  $0.25 \leq \omega_p \leq 14$  days and  $2 \leq \omega_r \leq 30$  days to prevent inferring unrealistically small  
468 or large values for these parameters for trajectories that were missing data prior to the peak and  
469 after the peak, respectively. We also constrained  $0 \leq \delta \leq 40$  as Ct values can only take values  
470 between 0 and the limit of detection (40).

471  
472 We next assumed that the observed  $\Delta Ct(t)$  could be described the following mixture model:

473

$$\Delta Ct(t) \sim \lambda \text{Normal}(E[\Delta Ct(t)], \sigma(t)) + (1 - \lambda) \text{Exponential}(\log(10)) \Big|_0^{\text{l.o.d}} \quad (\text{S4})$$

474

475  
476 where  $E[\Delta Ct(t)] = \text{l.o.d.} - E[Ct(t)]$  and  $\lambda$  is the sensitivity of the q-PCR test, which we fixed at 0.99.  
477 The bracket term on the right-hand side of the equation denotes that the distribution was truncated  
478 to ensure Ct values between 0 and the limit of detection. This model captures the scenario where  
479 most observed Ct values are normally distributed around the expected trajectory with standard  
480 deviation  $\sigma(t)$ , yet there is a small (1%) probability of an exponentially distributed false negative  
481 near the limit of detection. The  $\log(10)$  rate of the exponential distribution was chosen so that 90%  
482 of the mass of the distribution sat below 1 Ct unit and 99% of the distribution sat below 2 Ct units,  
483 ensuring that the distribution captures values distributed at or near the limit of detection. We did  
484 not estimate values for  $\lambda$  or the exponential rate because they were not of interest in this study;  
485 we simply needed to include them to account for some small probability mass that persisted near  
486 the limit of detection to allow for the possibility of false negatives.

487  
488 We used a hierarchical structure to describe the distributions of  $\omega_p$ ,  $\omega_r$ , and  $\delta$  for each person  
489 based on their respective population means  $\mu_{\omega_p}$ ,  $\mu_{\omega_r}$ , and  $\mu_{\delta}$  and population standard deviations  
490  $\sigma_{\omega_p}$ ,  $\sigma_{\omega_r}$ , and  $\sigma_{\delta}$  such that

491  
492  $\omega_p \sim \text{Normal}(\mu_{\omega_p}, \sigma_{\omega_p})$  (S5)  
493  $\omega_r \sim \text{Normal}(\mu_{\omega_r}, \sigma_{\omega_r})$   
494  $\delta \sim \text{Normal}(\mu_{\delta}, \sigma_{\delta})$

495  
496 We inferred population means ( $\mu$ ) separately for individuals infected with alpha, delta, and non-  
497 VOI/VOCs, as well as for unvaccinated and vaccinated individuals in a separate analysis. We  
498 used a Hamiltonian Monte Carlo fitting procedure implemented in Stan (version 2.24)<sup>19</sup> and R  
499 (version 3.6.2)<sup>37</sup> to estimate the individual-level parameters  $\omega_p$ ,  $\omega_r$ ,  $\delta$ , and  $t_p$  as well as the  
500 population-level parameters  $\sigma^*$ ,  $\mu_{\omega_p}$ ,  $\mu_{\omega_r}$ ,  $\mu_{\delta}$ ,  $\sigma_{\omega_p}$ ,  $\sigma_{\omega_r}$ , and  $\sigma_{\delta}$ . We used the following priors:

501  
502 *Hyperparameters:*

503  
504  $\sigma^* \sim \text{Cauchy}(0, 5) [0, \infty]$  (S6)

505  
506  $\mu_{\omega_p} \sim \text{Normal}(2.7, 14/6) [0.25, 14]$   
507  $\mu_{\omega_r} \sim \text{Normal}(7.4, 30/6) [2, 30]$  (S7)

508  $\mu_{\delta} \sim \text{Normal}(20, 40/6) [0, 40]$ .

509  
510  $\sigma_{\omega_p} \sim \text{Cauchy}(0, 14/\tan(\pi(0.95-0.5))) [0, \infty]$  (S8)

511  $\sigma_{\omega_r} \sim \text{Cauchy}(0, 30/\tan(\pi(0.95-0.5))) [0, \infty]$

512  $\sigma_{\delta} \sim \text{Cauchy}(0, 40/\tan(\pi(0.95-0.5))) [0, \infty]$

513  
514 *Individual-level parameters:*

515  $\omega_p \sim \text{Normal}(\mu_{\omega_p}, \sigma_{\omega_p}) [0.25, 14]$

516  $\omega_r \sim \text{Normal}(\mu_{\omega_r}, \sigma_{\omega_r}) [2, 30]$  (S9)

517  $\delta \sim \text{Normal}(\mu_{\delta}, \sigma_{\delta}) [0, 40]$

518  $t_p \sim \text{Normal}(0, 2)$

519  
520 The values in square brackets denote truncation bounds for the distributions. We chose a vague  
521 half-Cauchy prior with scale 5 for the observation variance  $\sigma^*$ . The priors for the population mean  
522 values ( $\mu$ .) are normally distributed priors spanning the range of allowable values for that  
523 parameter; this prior is vague but expresses a mild preference for values near the posterior  
524 estimates obtained from a previous analysis.<sup>38</sup> The priors for the population standard deviations  
525 ( $\sigma$ .) are half Cauchy-distributed with scale chosen so that 90% of the distribution sits below the  
526 maximum value for that parameter; this prior is vague but expresses a mild preference for  
527 standard deviations close to 0.

528  
529 We ran four MCMC chains for 2,000 iterations each with a target average proposal acceptance  
530 probability of 0.8. The first half of each chain was discarded as the warm-up. The Gelman R-hat  
531 statistic was less than 1.1 for all parameters. This indicates good overall mixing of the chains.  
532 There were no divergent iterations, indicating good exploration of the parameter space. The  
533 posterior distributions for  $\mu_{\delta}$ ,  $\mu_{\omega_p}$ , and  $\mu_{\omega_r}$ , were estimated separately for individuals infected with  
534 alpha, delta, and non-VOI/VOCs as well as for vaccinated and unvaccinated individuals. These  
535 are depicted in **Figure 1** (main text). Draws from the individual posterior viral trajectory  
536 distributions are depicted in **Supplementary Figures 1-11**. The mean posterior viral trajectories  
537 for each person are depicted in **Supplementary Figure 12**.

538  
539 Assessing sensitivity to different priors.

540 To ensure that our findings were not overly influenced by the prior distributions, we re-fit the model  
541 using two different sets of priors. The first “vague” set used posterior population means for  $\mu_{\omega p}$ ,  
542  $\mu_{\omega r}$ , and  $\mu_{\delta}$  chosen to lie near the center of the allowable range for those parameters. These priors  
543 were defined by

$$\begin{aligned} 544 & \mu_{\omega p} \sim \text{Normal}(14/2, 14/6) [0.25, 14] \\ 545 & \mu_{\omega r} \sim \text{Normal}(30/2, 30/6) [2, 30] \\ 546 & \mu_{\delta} \sim \text{Normal}(40/2, 40/6) [0, 40] \end{aligned} \tag{S10}$$

548  
549 The second set used unrealistically low prior means for  $\mu_{\omega p}$ ,  $\mu_{\omega r}$ , and  $\mu_{\delta}$  to check model robustness  
550 to highly biased prior distributions. These priors were defined by

$$\begin{aligned} 551 & \mu_{\omega p} \sim \text{Normal}(0, 14/6) [0.25, 14] \\ 552 & \mu_{\omega r} \sim \text{Normal}(0, 30/6) [2, 30] \\ 553 & \mu_{\delta} \sim \text{Normal}(20, 40/6) [0, 40]. \end{aligned} \tag{S11}$$

554  
555  
556 Note that we updated the prior means but kept the prior variances at their original wide values to  
557 avoid encoding over-confidence in the priors into the model. The posterior population means for  
558 these new sets of priors are depicted in **Supplementary Figures 13-14** (compare to **Figures 2-**  
559 **3**). Overall, the findings were consistent across choices of prior.

560

	<b>Minimum Ct</b>	<b>Maximum viral concentration (log<sub>10</sub> RNA copies/ml)</b>	<b>Proliferation duration (days)</b>	<b>Clearance duration (days)</b>	<b>Acute infection duration (days)</b>
<b>Non-VOI/VOC</b>	20.1 [18.3, 21.7]	8.2 [7.7, 11.6]	4.2 [3.3, 5.2]	7.3 [6.1, 8.4]	11.4 [10.1, 12.8]
<b>Alpha</b>	21.0 [19.1, 20.9]	7.9 [8.0, 11.5]	3.4 [2.6, 4.5]	6.2 [5.2, 7.4]	9.6 [8.3, 11.1]
<b>Delta</b>	19.8 [18.0, 22.0]	8.3 [7.7, 11.6]	3.0 [2.2, 4.0]	6.2 [5.2, 7.4]	9.2 [8.0, 10.6]
<b>Unvaccinated</b>	20.7 [19.8, 20.2]	8.0 [8.2, 11.5]	3.5 [3.0, 4.0]	7.5 [6.8, 8.2]	11.0 [10.3, 11.8]
<b>Vaccinated</b>	20.5 [19.0, 21.0]	8.1 [7.9, 11.5]	3.2 [2.5, 4.0]	5.5 [4.6, 6.5]	8.7 [7.6, 9.9]

561

562

563 **Supplementary Table 1. Posterior population viral trajectory parameters for SARS-CoV-2 infections**  
564 **by variant and vaccination status.** Reported values represent the posterior mean and 95% credible  
565 intervals (brackets) for each parameter.

566

567

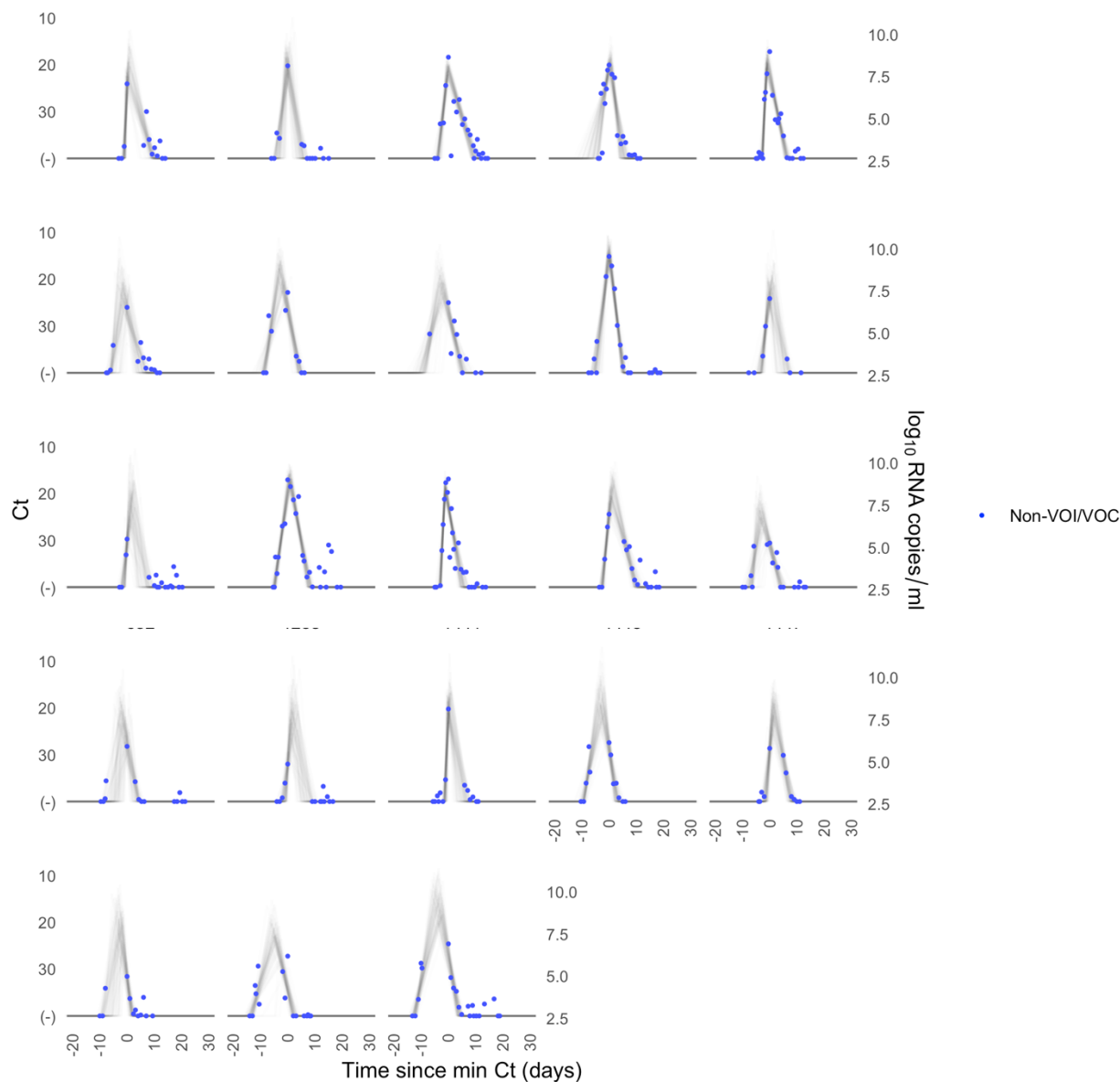
Standard (copies/ul)	Replicate 1 (Ct)	Replicate 2 (Ct)	Average Ct
10 <sup>6</sup>	19.3	19.7	19.5
10 <sup>5</sup>	23.0	21.2	22.1
10 <sup>4</sup>	26.9	26.7	26.8
10 <sup>3</sup>	30.6	30.4	30.5
10 <sup>2</sup>	34.0	34.0	34.0
10 <sup>1</sup>	37.2	36.6	36.9
10 <sup>0</sup>	N/A	39.9	39.9

568

569 **Supplementary Table 2. Standard curve relationship between virus RNA copies and Ct values.**  
570 Synthetic T7 RNA transcripts corresponding to a 1,363 base pair segment of the SARS-CoV-2 nucleocapsid  
571 gene were serially diluted from 10<sup>6</sup>-10<sup>0</sup> and evaluated in duplicate with RT-qPCR. The best-fit linear  
572 regression of the average Ct on the log<sub>10</sub>-transformed standard values had slope -3.60971 and intercept  
573 40.93733 (R<sup>2</sup> = 0.99).  
574



575



576

577

578 **Supplementary Figure 1. Ct values and estimated trajectories for non-VOI/VOIC SARS-CoV-2 infections (1/3).**

579 Each pane depicts the recorded Ct values (points) and derived log-10 genome equivalents per

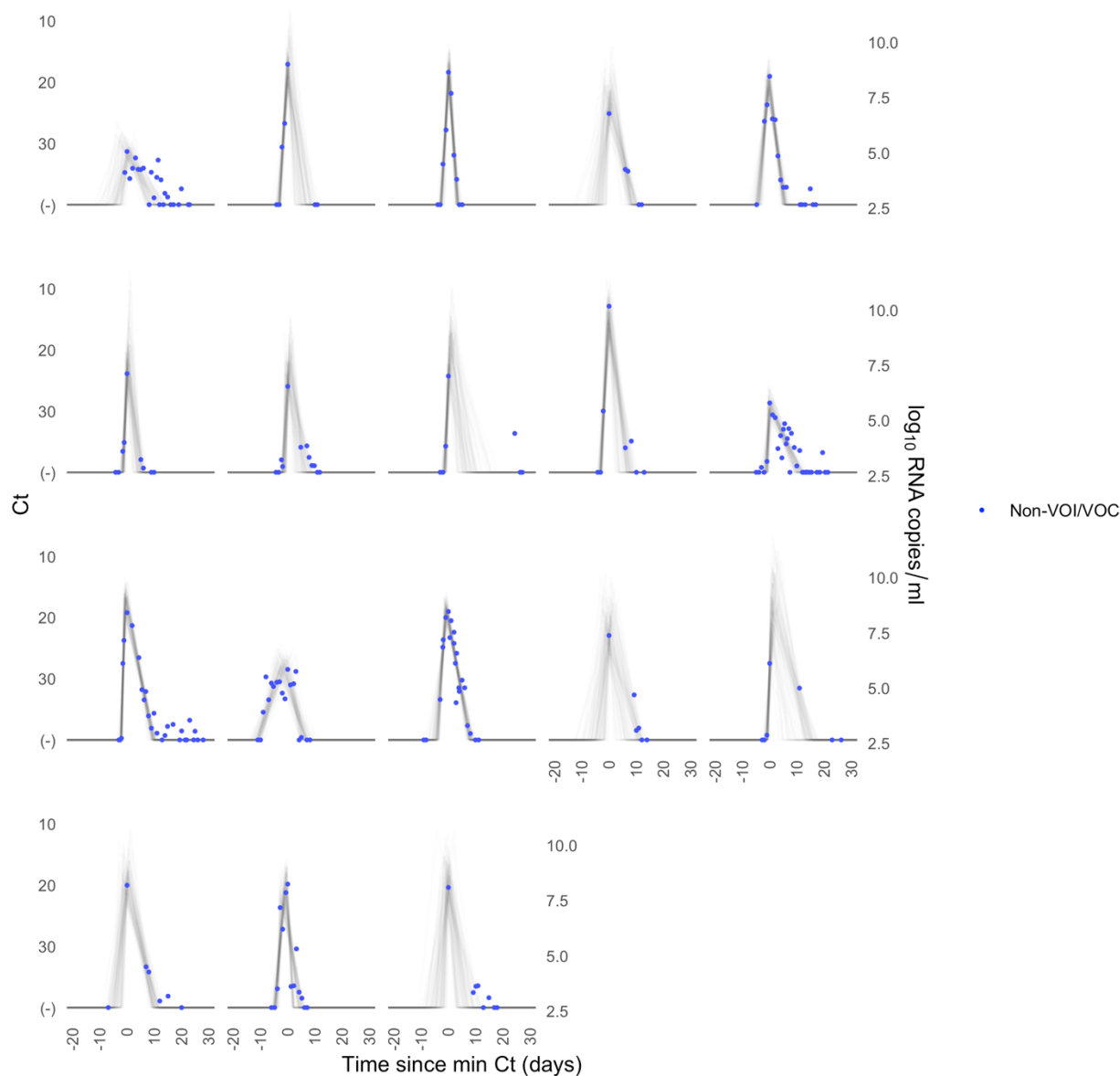
580 ml ( $\log_{10}(\text{ge/ml})$ ) for a single person during the study period. Points along the horizontal axis represent neg-

581 ative tests. Time is indexed in days since the minimum recorded Ct value (maximum viral concentration).

582 Lines depict 100 draws from the posterior distribution for each person's viral trajectory. Shaded boxes de-

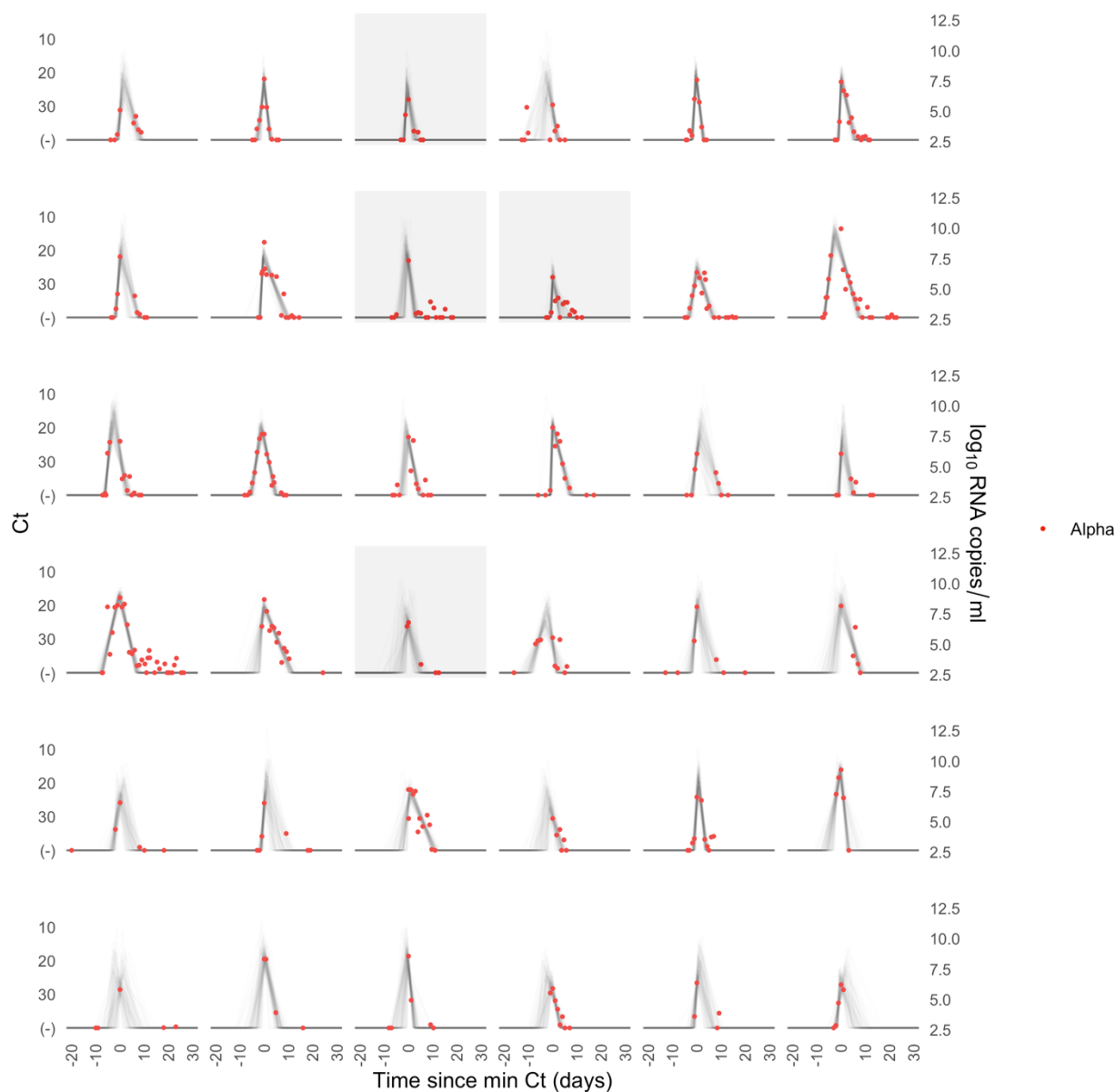
583 note breakthrough infections.

584



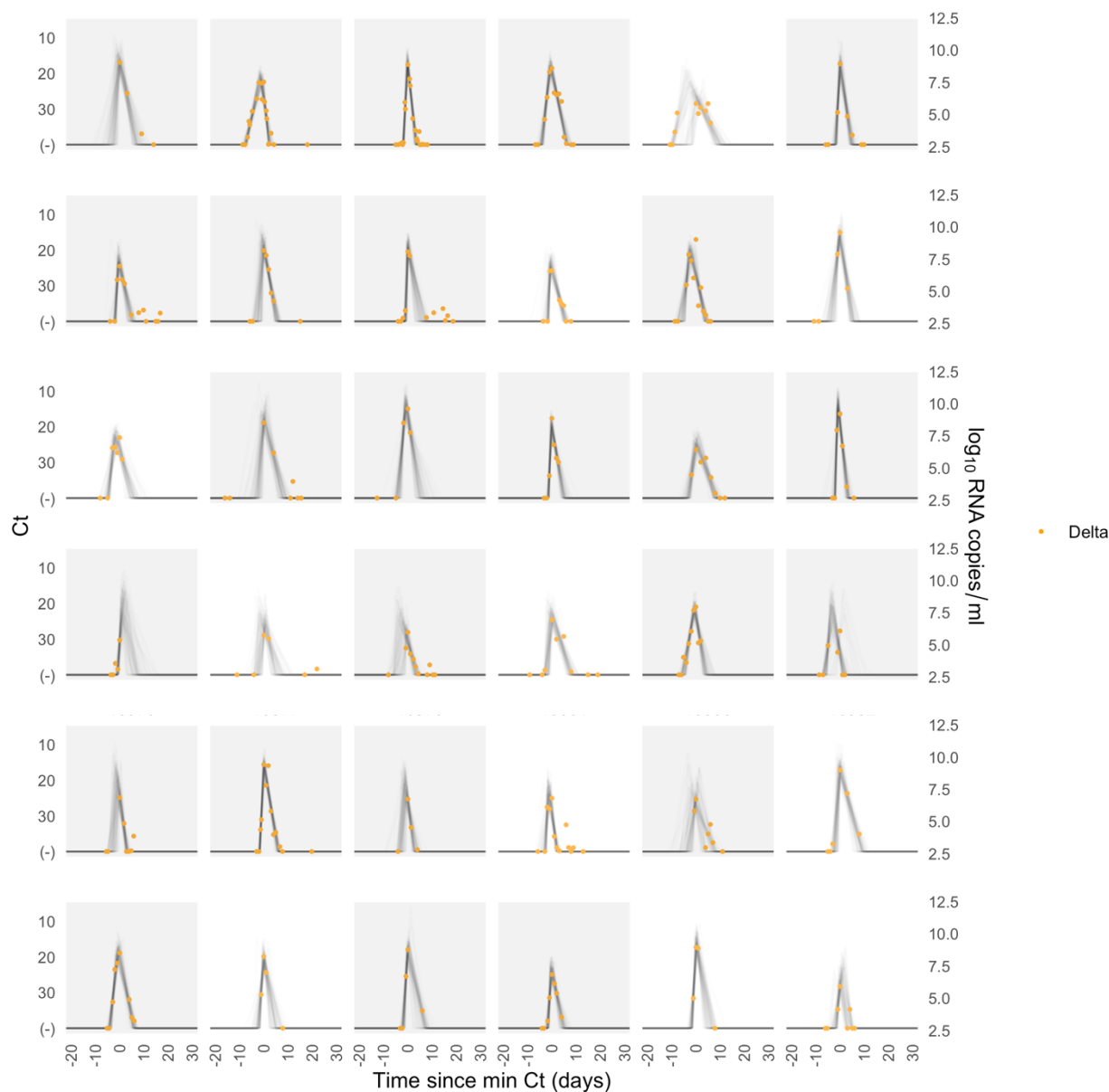
585  
586  
587  
588  
589  
590  
591  
592  
593  
594  
595  
596  
597  
598

**Supplementary Figure 2. Ct values and estimated trajectories for non-VOI/VOIC SARS-CoV-2 infections (2/3).** Each pane depicts the recorded Ct values (points) and derived log-10 genome equivalents per ml ( $\log(\text{ge/ml})$ ) for a single person during the study period. Points along the horizontal axis represent negative tests. Time is indexed in days since the minimum recorded Ct value (maximum viral concentration). Lines depict 100 draws from the posterior distribution for each person's viral trajectory. Shaded boxes denote breakthrough infections.



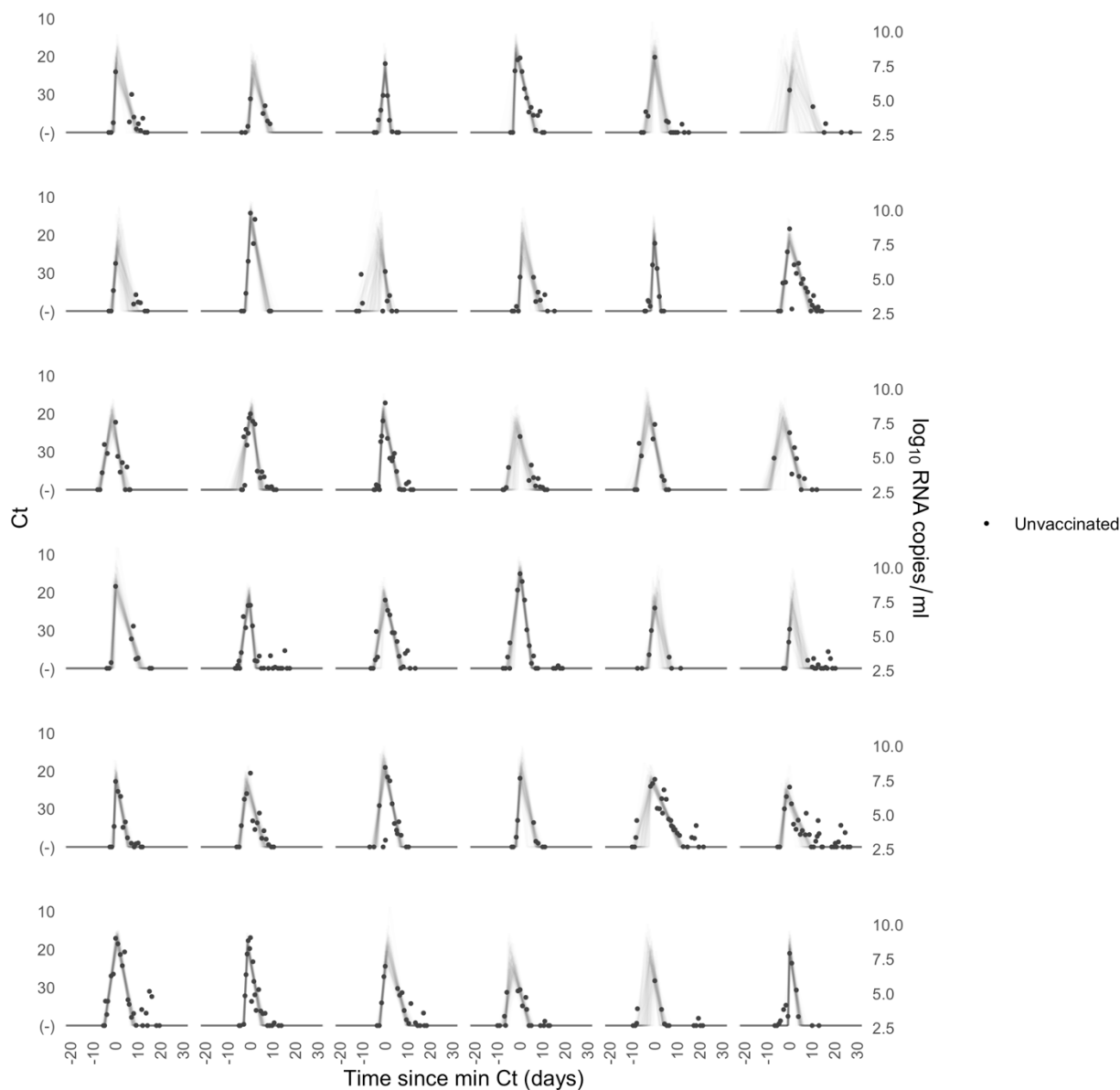
599  
600  
601  
602  
603  
604  
605  
606  
607  
608

**Supplementary Figure 3. Ct values and estimated trajectories for alpha SARS-CoV-2 infections.** Each pane depicts the recorded Ct values (points) and derived log-10 genome equivalents per ml ( $\log_{10}(\text{ge/ml})$ ) for a single person during the study period. Points along the horizontal axis represent negative tests. Time is indexed in days since the minimum recorded Ct value (maximum viral concentration). Lines depict 100 draws from the posterior distribution for each person's viral trajectory. Shaded boxes denote breakthrough infections.



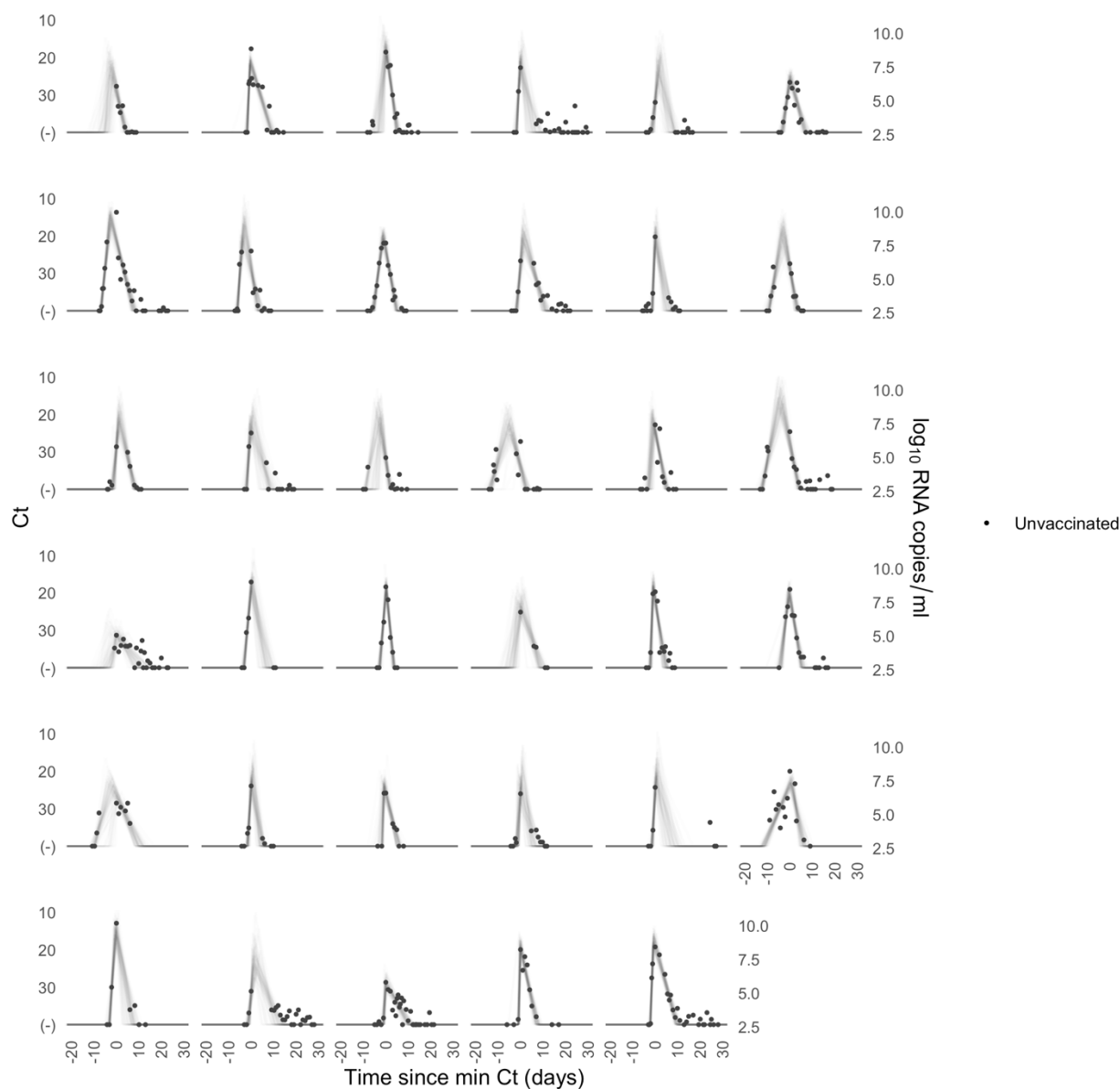
609  
610  
611  
612  
613  
614  
615  
616  
617

**Supplementary Figure 4. Ct values and estimated trajectories for delta SARS-CoV-2 infections.** Each pane depicts the recorded Ct values (points) and derived log-10 genome equivalents per ml (log<sub>10</sub>(ge/ml)) for a single person during the study period. Points along the horizontal axis represent negative tests. Time is indexed in days since the minimum recorded Ct value (maximum viral concentration). Lines depict 100 draws from the posterior distribution for each person's viral trajectory. Shaded boxes denote breakthrough infections.

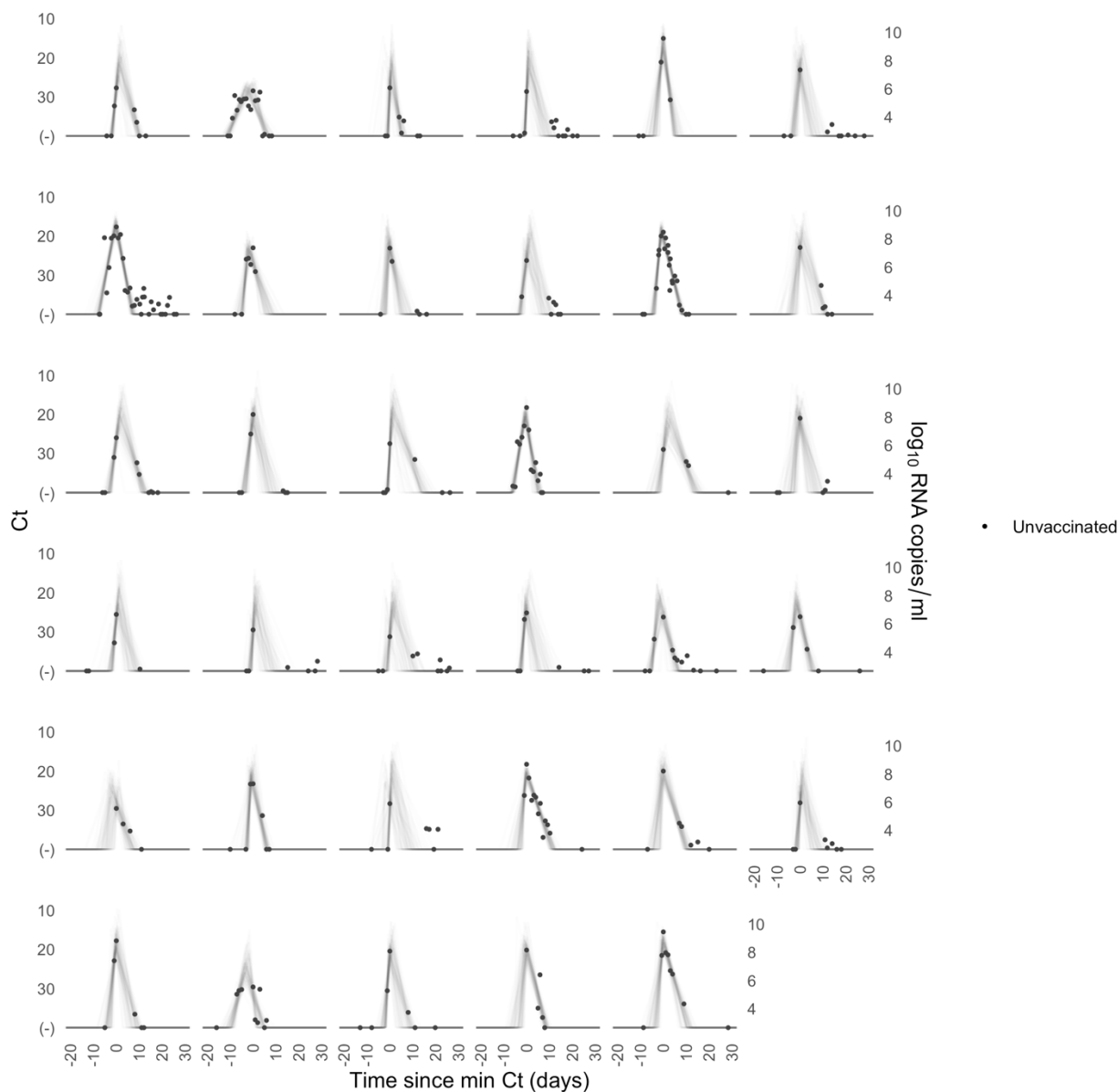


618  
619  
620  
621  
622  
623  
624  
625

**Supplementary Figure 5. Ct values and estimated trajectories for SARS-CoV-2 infections in unvaccinated individuals (1/4).** Each pane depicts the recorded Ct values (points) and derived log-10 genome equivalents per ml ( $\log(\text{ge/ml})$ ) for a single person during the study period. Points along the horizontal axis represent negative tests. Time is indexed in days since the minimum recorded Ct value (maximum viral concentration). Lines depict 100 draws from the posterior distribution for each person's viral trajectory.



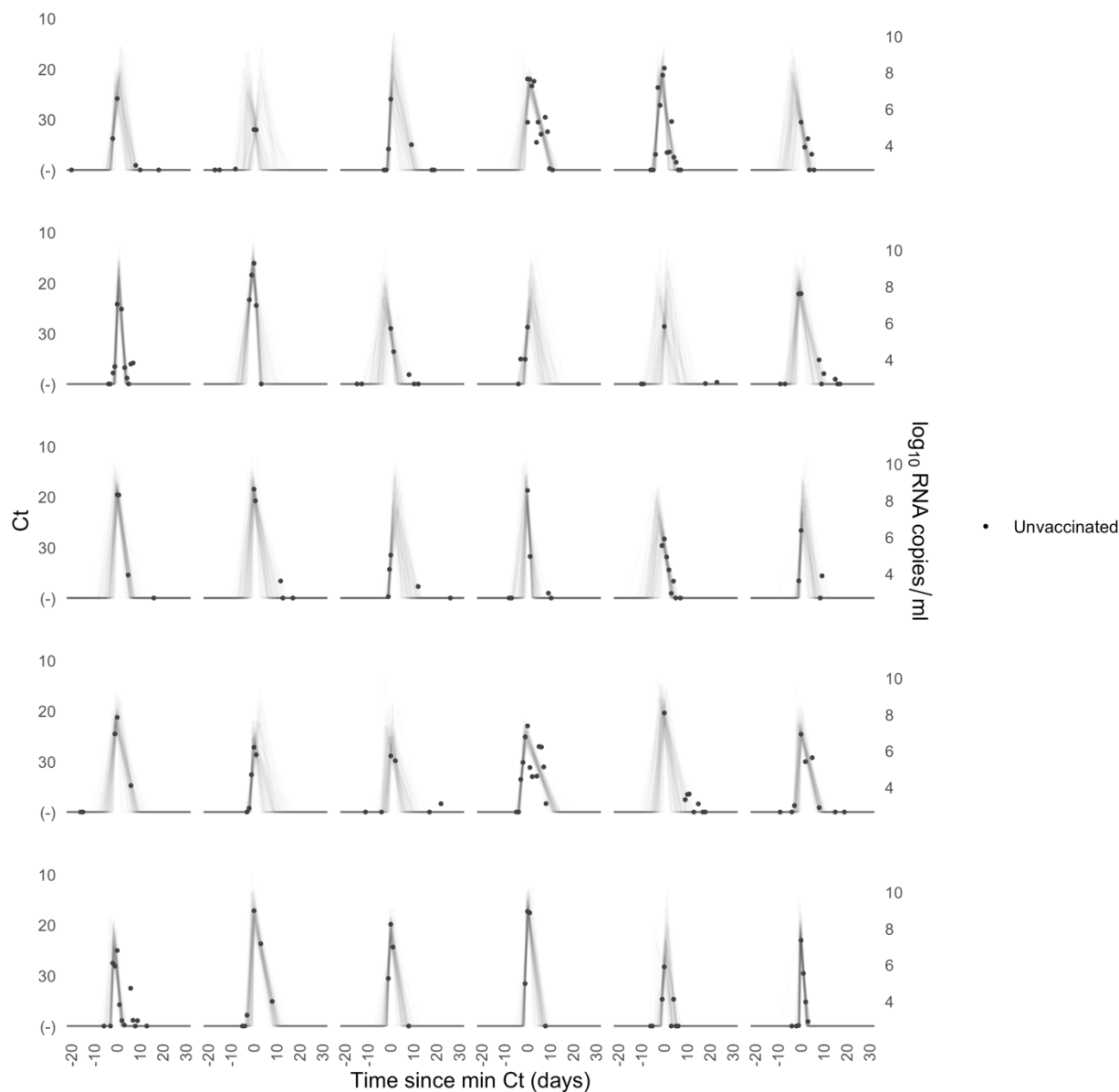
**Supplementary Figure 6. Ct values and estimated trajectories for SARS-CoV-2 infections in unvaccinated individuals (2/4).** Each pane depicts the recorded Ct values (points) and derived log-10 genome equivalents per ml ( $\log_{10}(\text{ge/ml})$ ) for a single person during the study period. Points along the horizontal axis represent negative tests. Time is indexed in days since the minimum recorded Ct value (maximum viral concentration). Lines depict 100 draws from the posterior distribution for each person's viral trajectory.



634  
635  
636  
637  
638  
639  
640  
641

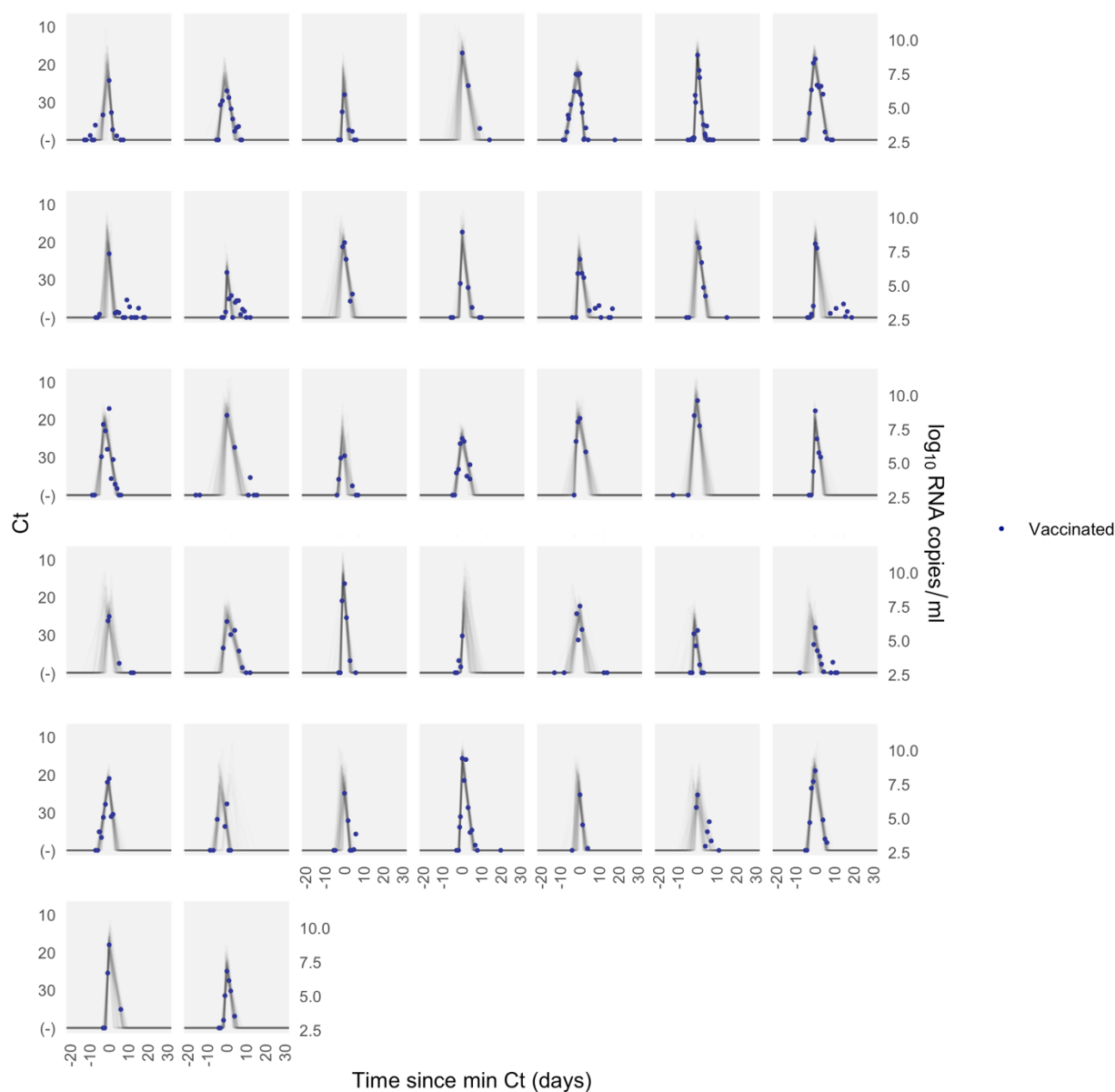
**Supplementary Figure 7. Ct values and estimated trajectories for SARS-CoV-2 infections in unvaccinated individuals (3/4).** Each pane depicts the recorded Ct values (points) and derived log-10 genome equivalents per ml ( $\log_{10}(\text{ge/ml})$ ) for a single person during the study period. Points along the horizontal axis represent negative tests. Time is indexed in days since the minimum recorded Ct value (maximum viral concentration). Lines depict 100 draws from the posterior distribution for each person's viral trajectory.





642  
643  
644  
645  
646  
647  
648  
649

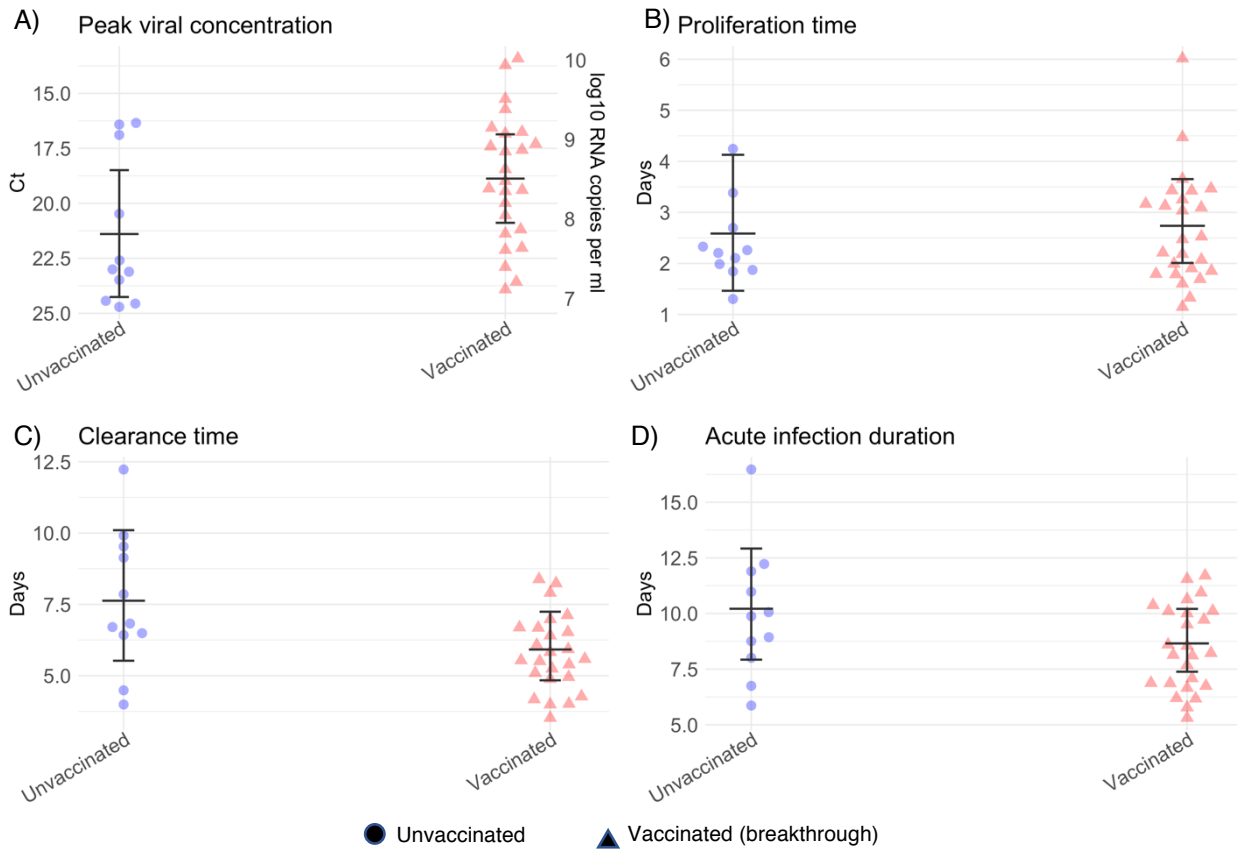
**Supplementary Figure 8. Ct values and estimated trajectories for SARS-CoV-2 infections in unvaccinated individuals (4/4).** Each pane depicts the recorded Ct values (points) and derived log-10 genome equivalents per ml ( $\log(\text{ge/ml})$ ) for a single person during the study period. Points along the horizontal axis represent negative tests. Time is indexed in days since the minimum recorded Ct value (maximum viral concentration). Lines depict 100 draws from the posterior distribution for each person's viral trajectory.



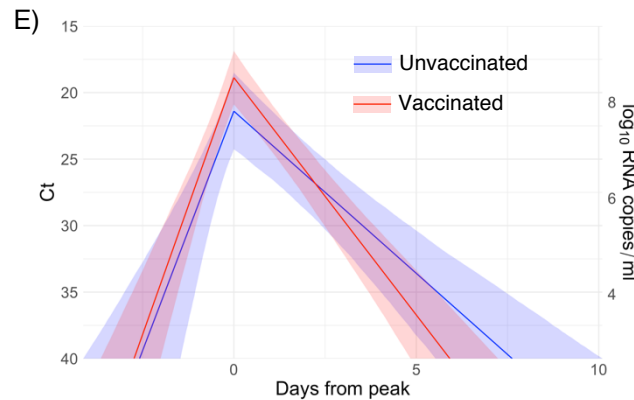
650  
651  
652  
653  
654  
655  
656  
657  
658

**Supplementary Figure 9. Ct values and estimated trajectories for SARS-CoV-2 infections in vaccinated individuals.** Each pane depicts the recorded Ct values (points) and derived log-10 genome equivalents per ml ( $\log(\text{ge/ml})$ ) for a single person during the study period. Points along the horizontal axis represent negative tests. Time is indexed in days since the minimum recorded Ct value (maximum viral concentration). Lines depict 100 draws from the posterior distribution for each person's viral trajectory. Shaded boxes denote breakthrough infections.

659

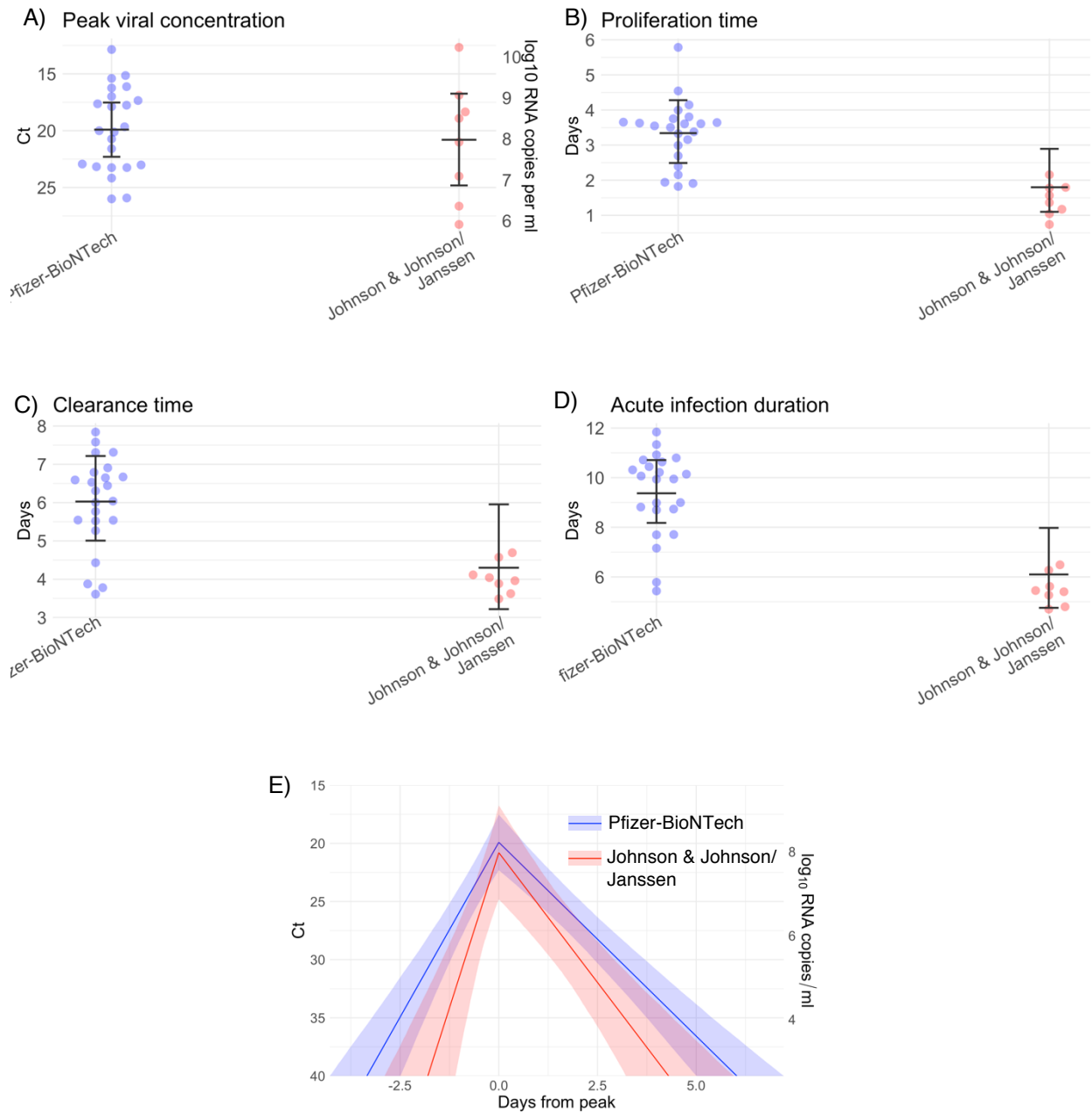


660  
661  
662  
663



664  
665  
666  
667  
668  
669  
670  
671  
672  
673  
674  
675  
676

**Supplementary Figure 10. Estimated viral trajectory parameters for vaccinated and unvaccinated individuals infected with SARS-CoV-2 variant delta.** Individual posterior means (points) with population means and 95% credible intervals (hatched lines) for (A) the peak viral concentration, (B) the proliferation duration, (C) the clearance duration, and (D) the total duration of acute infection for unvaccinated (blue) and vaccinated (red) individuals infected with delta. Circles denote unvaccinated individuals and triangles denote vaccinated individuals (breakthroughs). The points are jittered horizontally to avoid overlap. Pane (E) depicts the mean posterior viral trajectories for unvaccinated (blue) vs. vaccinated (red) individuals, as specified by the population means and credible intervals in (A)-(D). Solid lines in pane (E) depict the mean posterior viral trajectories and shaded regions represent 95% credible areas for the mean posterior trajectories.



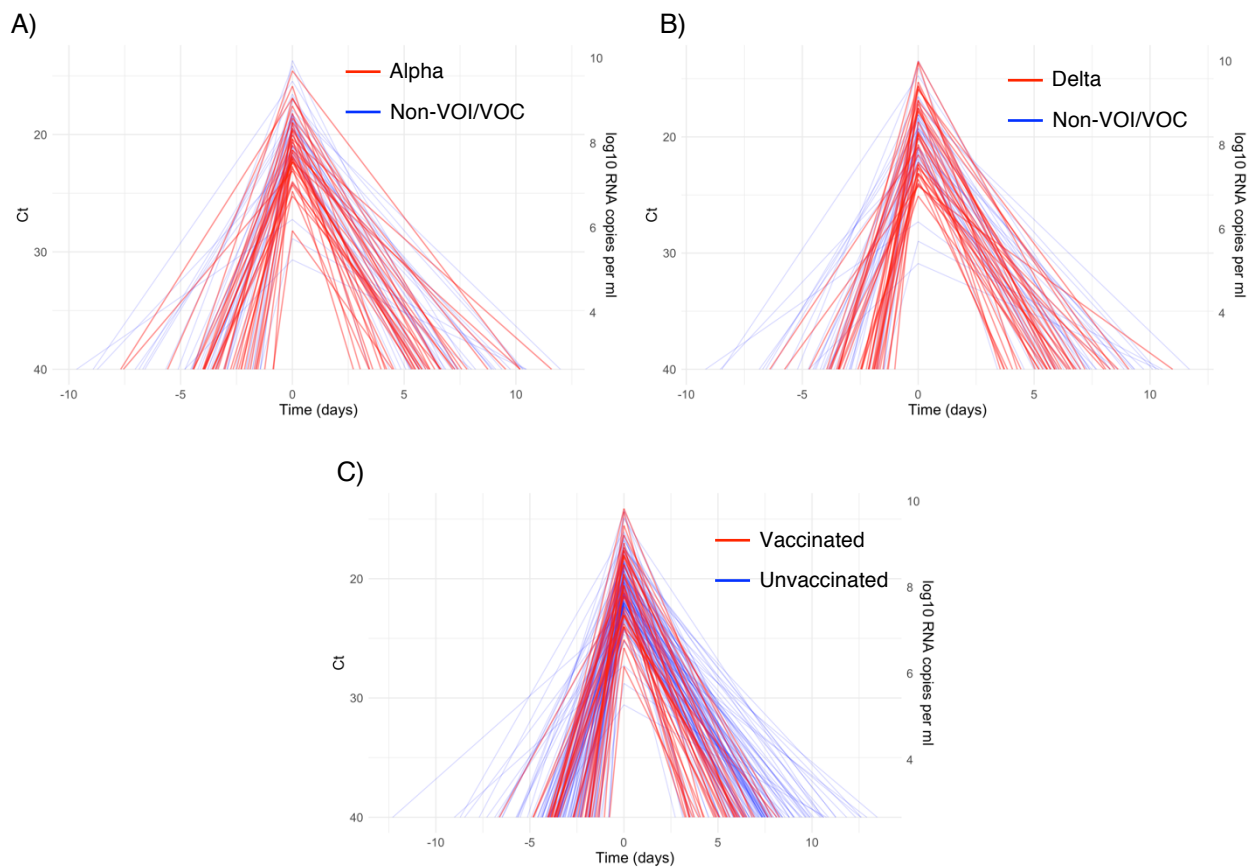
677  
678

679  
680

681  
682  
683  
684  
685  
686  
687  
688  
689  
690  
691  
692  
693  
694  
695

**Supplementary Figure 11. Estimated viral trajectory parameters for individuals vaccinated with the Pfizer-BioNTech vaccine vs. the Johnson & Johnson/Janssen vaccine.** Individual posterior means (points) with population means and 95% credible intervals (hatched lines) for (A) the peak viral concentration, (B) the proliferation duration, (C) the clearance duration, and (D) the total duration of acute infection for breakthrough infections in individuals vaccinated with the Pfizer-BioNTech vaccine (blue) and the Johnson & Johnson/Janssen vaccine (red). The points are jittered horizontally to avoid overlap. Pane (E) depicts the mean posterior viral trajectories for breakthrough infections in individuals vaccinated with the Pfizer-BioNTech vaccine (blue) vs. the Johnson & Johnson/Janssen vaccine (red), as specified by the population means and credible intervals in (A)-(D). Solid lines in pane (E) depict the mean posterior viral trajectories and shaded regions represent 95% credible areas for the mean posterior trajectories.

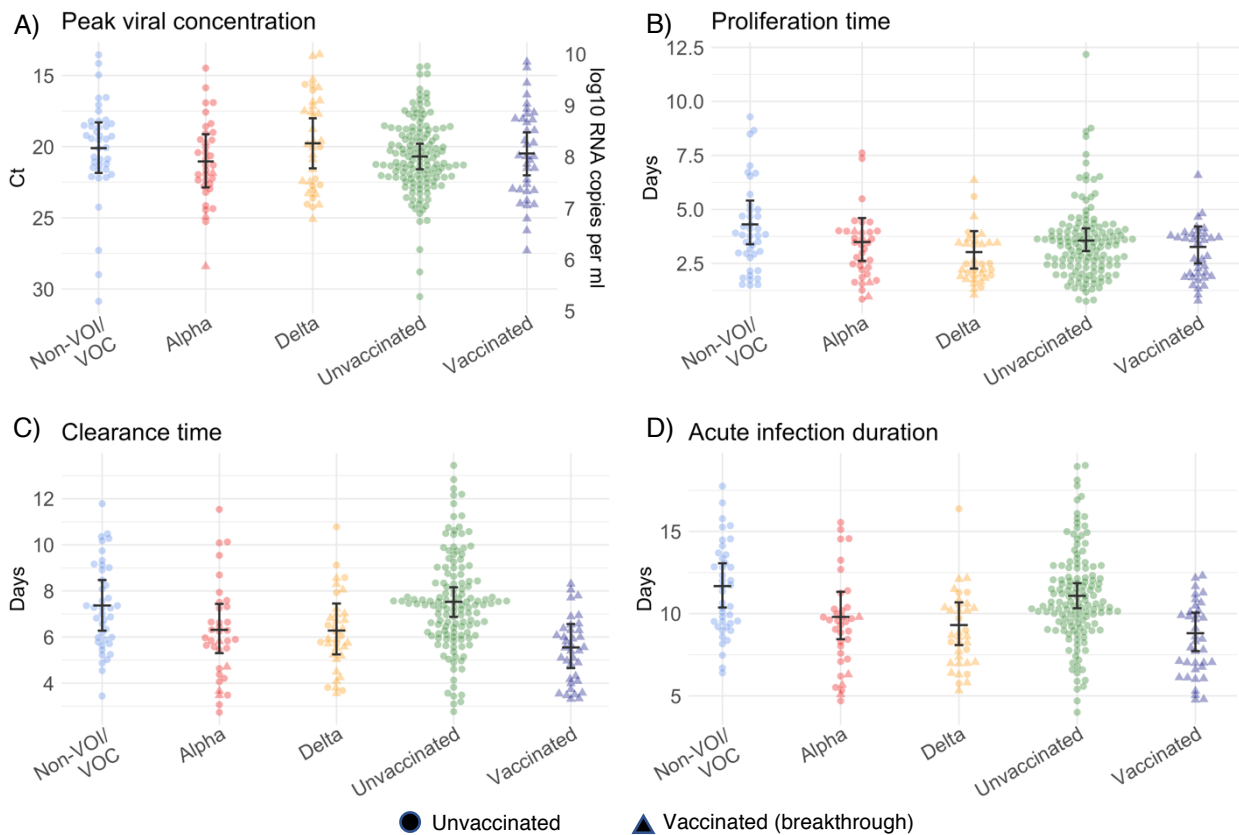
696  
697



698  
699  
700

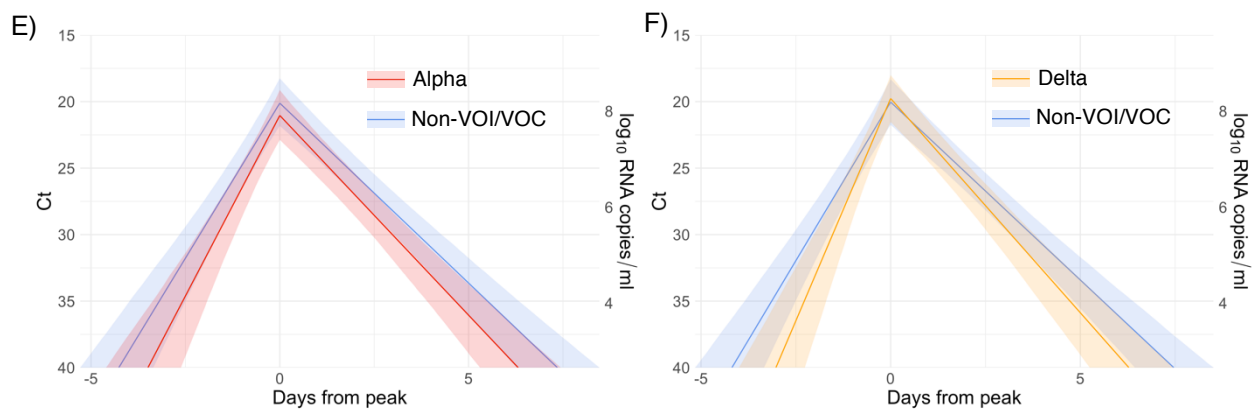
701  
702  
703  
704  
705  
706  
707  
708

**Supplementary Figure 12. Mean posterior viral trajectories for each person.** Pane (A) depicts alpha infections (red) against non-VOI/VOC infections (blue). Pane (B) depicts delta infections (red) against non-VOI/VOC infections (blue). Pane (C) depicts infections in vaccinated people (red) against unvaccinated people (blue). Trajectories are aligned temporally to have the same peak time.

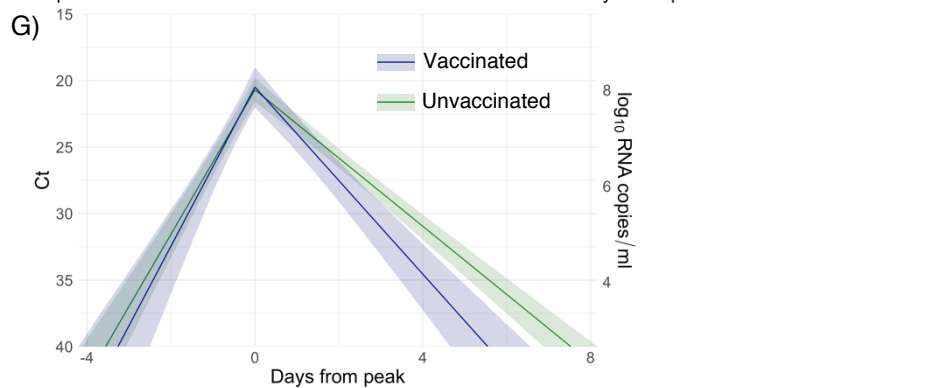


709

710  
711  
712  
713



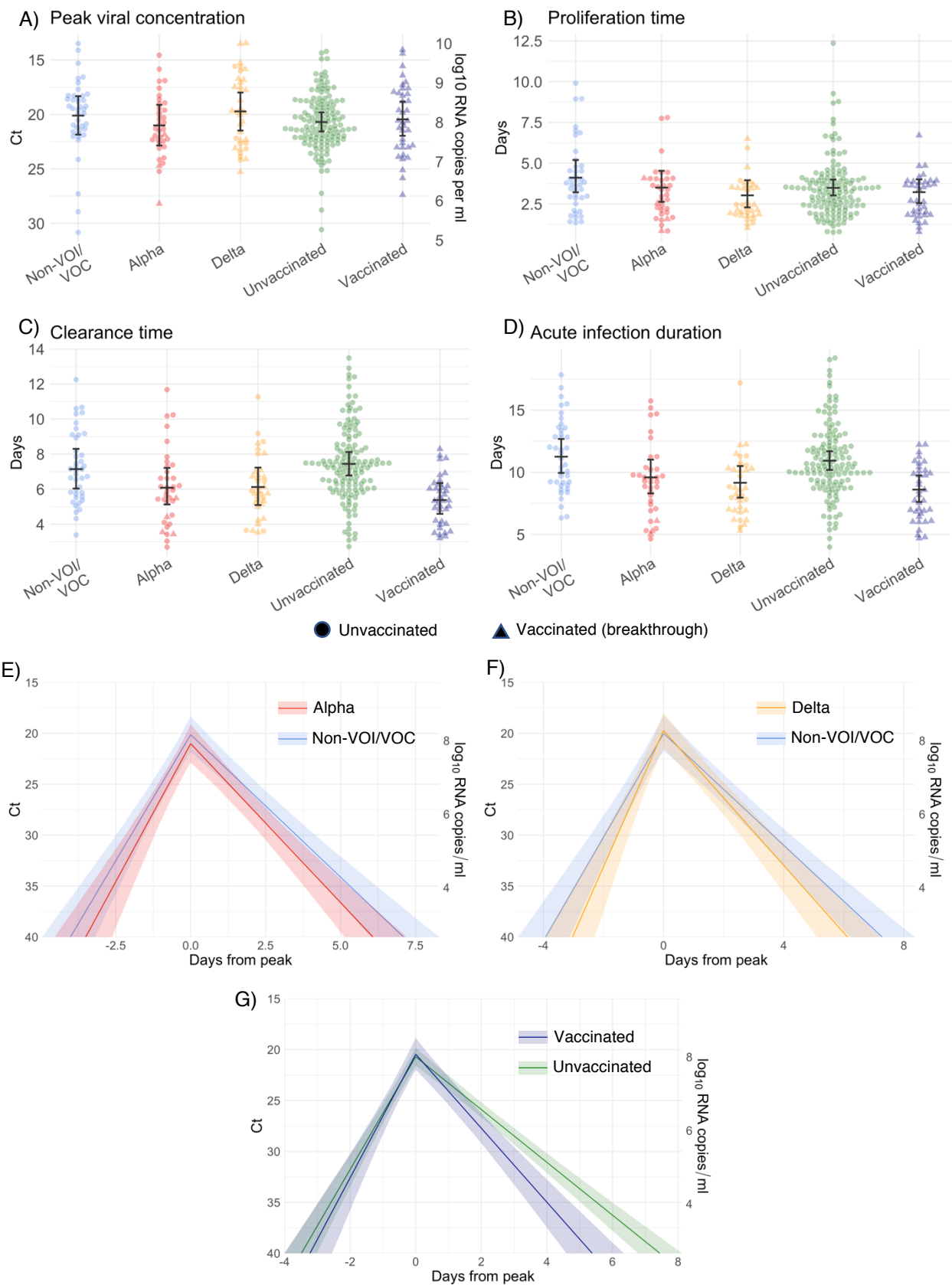
714



715  
716

717 **Supplementary Figure 13. Estimated viral trajectory parameters for SARS-CoV-2 infections by vari-**  
718 **ant and vaccination status using uninformative priors.** Individual posterior means (points) with popula-  
719 tion means and 95% credible intervals (hatched lines) for (A) the peak viral concentration, (B) the prolifer-  
720 ation duration, (C) the clearance duration, and (D) the total duration of acute infection for individuals infected  
721 with a non-VOI/VOC (blue), alpha (red), or delta (purple), and for individuals who were unvaccinated (green)  
722 or vaccinated (maroon). Circles denote unvaccinated individuals and triangles denote vaccinated individu-  
723 als (breakthroughs). The points are jittered horizontally to avoid overlap. Solid lines in panes (E)-(F) depict  
724 the mean posterior viral trajectories for alpha (E, red) and delta (F, purple) infections respectively relative  
725 to non-VOI/VOC infections (blue), as specified by the population means and credible intervals in (A)-(D).  
726 Solid lines in pane (G) depict the mean posterior viral trajectory for vaccinated (maroon) relative to unvac-  
727 cinated (green) individuals. The shaded regions in (E)-(G) represent 95% credible areas for the mean pop-  
728 ulation trajectories. Priors were informed by a previous analysis and are defined in Eq. (S10).  
729





730

731  
732  
733

734  
735

736  
737

738 **Supplementary Figure 14 Estimated viral trajectory parameters for SARS-CoV-2 infections by vari-**  
739 **ant and vaccination status using biased (low) priors.** Individual posterior means (points) with population  
740 means and 95% credible intervals (hatched lines) for (A) the peak viral concentration, (B) the proliferation  
741 duration, (C) the clearance duration, and (D) the total duration of acute infection for individuals infected with  
742 a non-VOI/VOC (blue), alpha (red), or delta (purple), and for individuals who were unvaccinated (green) or  
743 vaccinated (maroon). Circles denote unvaccinated individuals and triangles denote vaccinated individuals  
744 (breakthroughs). The points are jittered horizontally to avoid overlap. Solid lines in panes (E)-(F) depict the  
745 mean posterior viral trajectories for alpha (E, red) and delta (F, purple) infections respectively relative to  
746 non-VOI/VOC infections (blue), as specified by the population means and credible intervals in (A)-(D). Solid  
747 lines in pane (G) depict the mean posterior viral trajectory for vaccinated (maroon) relative to unvaccinated  
748 (green) individuals. The shaded regions in (E)-(G) represent 95% credible areas for the mean population  
749 trajectories. Priors were chosen to be unrealistically low and are defined in Eq. (S11).  
750